The NALCN channel complex is voltage sensitive and directly modulated by extracellular calcium

H. C. Chua[1], M. Wulf[1], C. Weidling[1], L. P. Rasmussen[1], S. A. Pless[1]*

[1]Department of Drug Design and Pharmacology, University of Copenhagen, Jagtvej 160, 2100 Copenhagen, Denmark.

* Corresponding author. Email: stephan.pless@sund.ku.dk

Abstract

The sodium leak channel (NALCN) is essential for survival in mammals: NALCN mutations are life-threatening in humans and knockout is lethal in mice. However, the basic functional and pharmacological properties of NALCN have remained elusive. Here, we found that the robust function of NALCN in heterologous systems requires co-expression of UNC79, UNC80 and FAM155A. The resulting NALCN channel complex is constitutively active, conducts monovalent cations but is blocked by physiological concentrations of extracellular divalent cations. Our data support the notion that NALCN is directly responsible for the increased excitability observed in a variety of neurons in reduced extracellular Ca^{2+}. Despite the smaller number of voltage-sensing residues in NALCN, the constitutive activity is modulated by voltage, suggesting that voltage-sensing domains can give rise to a broader range of gating phenotypes than previously anticipated. Our work points towards formerly unknown contributions of NALCN to neuronal excitability and opens avenues for pharmacological targeting.

Introduction

Many neurons display a basal Na^+ conductance at rest that is involved in the regulation of resting membrane potential (RMP), spontaneous firing and pacemaking activity (*1-3*). The sodium leak channel (NALCN) contributes to this tonic current in certain types of neurons and plays a critical role in their excitability (*4-9*). There are now multiple lines of evidence in support of the physiological significance of NALCN. Firstly, NALCN knockout is lethal within a day after birth in mice due to disrupted respiratory rhythm (*4*). Secondly, changes in NALCN expression and/or function have been implicated in other physiological processes such as motor function, pain sensitivity and circadian rhythm in animals (*6, 10-14*). Lastly, accumulating evidence shows that mutations in NALCN cause severe congenital neurodevelopmental disorders in humans (*15, 16*).

NALCN represents the sole member of a distinct branch of the four-domain ion channel family, which includes the extensively studied voltage-gated sodium and calcium channels (Na_Vs and Ca_Vs) (*17*). These channels are made up of four homologous domains (DI–IV), each with six transmembrane segments (S1–S6). Functionally, the voltage-sensing domains (VSDs), formed by S1–S4 of each domain, detect changes in membrane potential and induce the opening or closing of the ion-conducting pore domain, formed by S5 and S6. Unlike Na_Vs and Ca_Vs, however, the fundamental functional and pharmacological properties of NALCN remain largely unexplored due to poor heterologous expression (*18-21*). In this study, we found that the robust functional expression of NALCN requires UNC79, UNC80 and FAM155A, three ubiquitous neuronal proteins that have been independently shown to interact with NALCN (*5, 11, 12, 22*). This enabled the first in-depth functional characterisation of the NALCN channel complex and unequivocally defines NALCN as permeable to small monovalent cations, but potently blocked by divalent cations through a direct pore-blocking mechanism. Furthermore, we show that NALCN does not form a simple Ohmic leak channel, but displays voltage-dependent gating mediated primarily by positive charges in the S4 of DI and II.

Results

Co-expression of NALCN, UNC79, UNC80 and FAM155A results in robust currents

Whether NALCN alone can generate leak currents in heterologous expression systems has remained a matter of debate (*4, 18-21, 23*). Here, we found that the expression of NALCN alone did not result in detectable responses to a wide range of voltage steps in HEK-293T cells or *Xenopus laevis* oocytes (Fig. 1A and S1). We thus set out to test if functional expression of NALCN, like that of some of the Ca_Vs (*24*), is dependent on the presence of additional auxiliary proteins. We found that functional expression of NALCN in both heterologous systems requires UNC79, UNC80 and FAM155A (Fig. 1A and S1). Furthermore, rat NALCN(*4*), human FAM155B and mouse FAM155A (*12*) orthologs can functionally substitute human NALCN and FAM155A, respectively (Fig. S1B). We also tested the effect of co-expressing FAM155A and FAM155B with NALCN, UNC79 and UNC80, but did not find any apparent functional differences (Fig. S1B). UNC79 and UNC80 are large, potentially disordered proteins (2635 and 3258 aa, respectively) that are highly conserved among animals (*25, 26*). They contain no recognisable functional domains, and their subcellular localisations remain unclear. By contrast, FAM155A (458 aa) contains at least one transmembrane segment and a conserved cysteine-rich domain (CRD) (*12, 27*). The *C. elegans* and mouse orthologues have previously been suggested to reside in the endoplasmic reticulum (ER) and facilitate NALCN trafficking. Here, however, we were able to co-immunoprecipitate UNC79, UNC80 and FAM155A with NALCN (Fig. S2B). Therefore, we refer to the NALCN-UNC79-UNC80-FAM155A combination as the NALCN channel complex henceforth.

In patch-clamp experiments, we found that HEK-293T cells expressing all components of the NALCN channel complex showed low seal resistances (R_m~100 MΩ) after breaking into whole-cell mode (Fig. S1D). Despite the low seal resistances, a feature typically associated with non-specific Ohmic leak current in electrophysiological studies (*20*), we observed clear voltage-dependent changes in current in response to both depolarising and hyperpolarising voltage steps, irrespective of the holding potential (HP) (Fig. 1A-B, S1A). The gating behaviour of the NALCN complex observed is unusual in a few aspects. First, we did not observe full channel closure within the tested voltage range, indicating that the complex is constitutively active (Fig. 1A-B). Second, the complex is differentially modulated by voltage, with depolarisation eliciting non-inactivating current and hyperpolarisation eliciting large inward currents that deactivate rapidly but incompletely. Third, the inward component during hyperpolarising steps is much more pronounced under symmetrical Na^+ condition than under more physiological condition (Fig. 1A-B), suggesting that ionic species can affect channel function. Fourth, a Na_V-like, bell-shaped I-V relationship between -100 to 0 mV, with a maximal inward current around -40 mV was detected for the NALCN complex under a more physiological recording condition (Fig. 1B). Overall, the gating phenotype is distinct from that of other canonical voltage-gated

ion channels (VGICs), which typically populate one or more closed (or inactivated) states upon hyper- or depolarisation. We also tested for potential involvement of Src family of kinases (SFKs) in the function of NALCN channel complex, as SFKs have been suggested to underlie NALCN activation (*22*). However, we found that neither the SFK activator peptide nor the SFK inhibitors (PP1 and SU 6656) showed any apparent functional effects during patch-clamping experiments (Fig. S1E-F), indicating that SFKs are not required for the NALCN-mediated currents observed in our study.

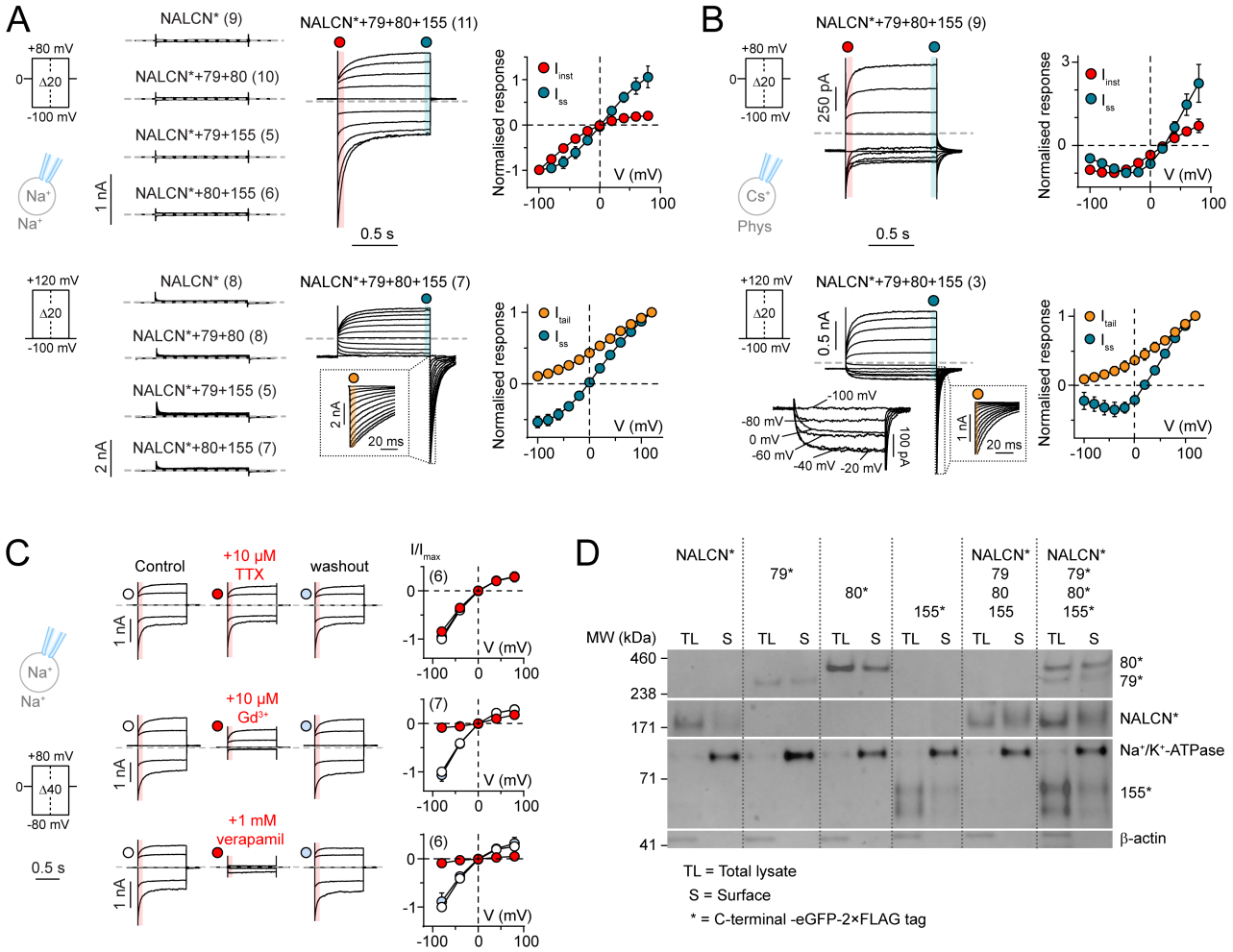

Fig. 1. Functional expression of NALCN requires UNC79, UNC80 and FAM155A. (A-B) Whole-cell patch-clamp recordings from HEK-293T cells expressing NALCN-eGFP-2×FLAG (NALCN*) alone, or in different combinations with UNC79 (79), UNC80 (80) and FAM155A (155) under (A) symmetrical Na^+ and (B) more physiological conditions using voltage-step protocols shown on the left. Normalised I-V plots highlighting the different current components of NALCN*+79+80+155 are shown on the right. The instantaneous current (I_{inst}; red) was measured in the beginning of a voltage step change, immediately after the transient current settled. The steady-state current (I_{ss}; blue) was measured at the end of a voltage step. Insets show tail currents (I_{tail};

orange) immediately after repolarisation to -100 mV. (C) Current responses (left) and I_{inst}-V plots (right, normalised to the control current) in the absence and presence of TTX, Gd^{3+} or verapamil under symmetrical Na^{+} condition. Data in A-C are shown as mean ± SD; grey dashed lines indicate 0 nA; numbers in parentheses indicate number of individual cells used for recordings. (D) Western blot of total lysate and surface fraction proteins extracted from HEK-293T cells expressing the indicated constructs (see also Fig. S2A).

Next, we investigated if the limited pharmacological profile established for NALCN thus far is preserved when the channel is co-expressed with UNC79, UNC80 and FAM155, i.e. insensitivity to TTX, inhibition by low micromolar concentrations of Gd^{3+} and high micromolar concentrations of the Ca_V inhibitor verapamil. We found that TTX application had no effect on current amplitude, while both Gd^{3+} and verapamil showed inhibitory effects (Fig. 1C). We also assessed the subcellular localisation of NALCN, UNC79, UNC80 and FAM155A, and found that all four proteins showed membrane localisation, both when expressed alone or together in HEK-293T cells (Fig. 1D and S2A). To determine functionally critical regions of these proteins, we expressed full-length NALCN with a series of truncated constructs for UNC79, UNC80 and FAM155A in *Xenopus laevis* oocytes and measured the resulting currents. We found that robust function required the presence of virtually full-length UNC79 and UNC80 proteins, although short truncations were tolerated at the C- and N-terminus, respectively (Fig. S3A-B). In the case of FAM155A, the presence of the first putative transmembrane domain and the CRD were absolutely required for function, while deletion of a second putative transmembrane domain was less detrimental (Fig. S3C). To determine if the lack of function was due to impaired cell surface expression, we also assessed the subcellular localisation of the truncated proteins. Somewhat surprisingly, we detected clear membrane localisation for all truncated constructs (Fig. S4). These results raise the possibility that UNC79, UNC80 and FAM155A are integral or peripheral membrane proteins that are at least in part exposed to the extracellular side of the cell membrane. However, given the current severe lack of knowledge on the topology of these proteins and the possibility that the -eGFP-2×FLAG tag may affect the subcellular localisation of fusion proteins, further studies are necessary to clarify these results in the future. Taken together, our data suggest that although NALCN can traffic to the membrane by itself, co-expression with UNC79, UNC80 and FAM155A is a prerequisite for the formation of a functional NALCN channel complex.

The NALCN channel complex is selective for monovalent cations

To define the ion selectivity profile of the NALCN channel complex, we first determined the current-carrying ions under bi-ionic conditions. We found that current directionality and reversal potentials (E_{rev}s) were sensitive to substitution of either extracellular or intracellular Na^+ with the large cation N-methyl-D-glucamine ($NMDG^+$), but not to replacement of extracellular Cl^- with the large anion methanesulfonate (MS^-) (Fig. 2A), consistent with permeability for cations and not anions. Next, we assessed the permeability of different cations (Li^+, K^+, Cs^+, TEA^+, Ca^{2+}, Mg^{2+} and Ba^{2+}) by having equimolar concentrations of test cations on the extracellular side (150 mM for monovalent cations (X^+); 110 mM for divalent cations (X^{2+})) and the impermeable $NMDG^+$ (150 mM) on the intracellular side. We observed voltage-dependent currents in the presence of extracellular Li^+, K^+ or Cs^+, but not with TEA^+ or X^{2+} (Ca^{2+}, Mg^{2+}, Ba^{2+}; Fig. 2B). The maximal current amplitudes of Li^+, K^+ and Cs^+ elicited at -80 mV, however, were smaller compared to Na^+ (57 ± 8 %, 89 ± 11 % and 76 ± 11 % of Na^+ current, respectively). To measure the E_{rev}s of the permeable cations, we ran a ramp protocol from -80 to +80 mV. The permeability ratios (P_{Na}/P_X) calculated based on the E_{rev}s revealed a permeability sequence of $Na^+ \approx Li^+ > K^+ > Cs^+$ (Fig. 2C). This permeability sequence was altered to $Na^+ \approx Li^+ \approx K^+ > Cs^+$ when the putative selectivity filter (SF) motif of NALCN (EEKE) was mutated to that of Na_Vs (DEKA; Fig. 2D).

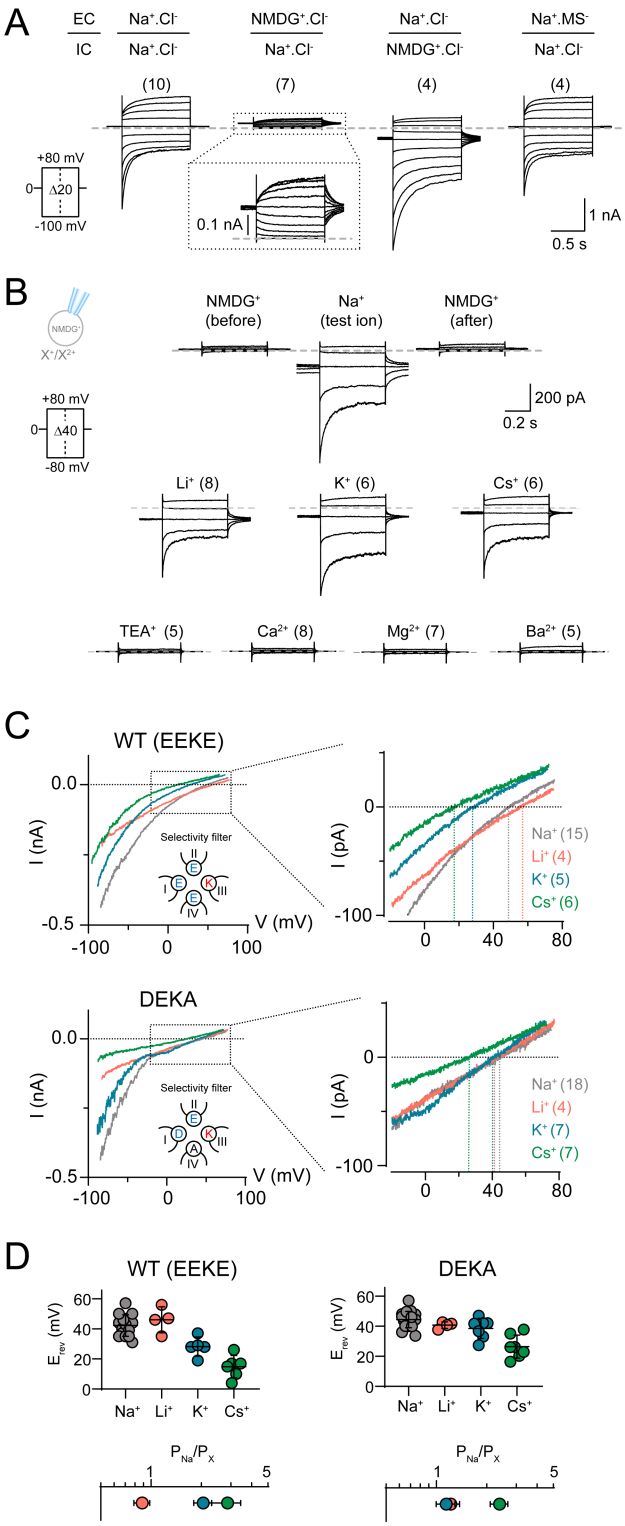

Fig. 2. The NALCN channel complex is selective for small monovalent cations. (A) Representative current traces of HEK-293T cells expressing NALCN*+79+80+155 under various bi-ionic conditions in response to the voltage protocol shown. EC=extracellular; IC=intracellular. (B) Representative current traces obtained with intracellular $NMDG^+$ and different

extracellular mono- or divalent cations using voltage-step protocols shown on the left. (C) The upper panel shows currents obtained with a voltage ramp protocol (-80 to 80 mV) with different test ions for both WT (EEKE SF, top) and the DEKA SF mutant (bottom) using intracellular $NMDG^+$ solution; insets show only -20 to +80 mV range. (D) Reversal potentials of different test ions and their permeability relative to Na^+; data shown as mean ± SD; grey dashed lines indicate 0 nA; numbers in parentheses indicate number of individual cells used for recordings.

The NALCN pore is blocked by extracellular divalent cations

To investigate if X^{2+} are merely impermeable or directly blocking the channel, we exposed cells to extracellular solutions containing 120 mM Na^+ in the absence and presence of 1 mM of Ca^{2+}, Mg^{2+} or Ba^{2+}. We found that all three X^{2+} inhibited Na^+ currents to varying degrees, with Ca^{2+} being the most potent, followed by Mg^{2+} and Ba^{2+} (83 ± 10 %, 59 ± 11 % and 37 ± 11 % inhibition of I_{inst} respectively; Fig. 3A). We also determined the sensitivity of Ca^{2+} inhibition by measuring current responses in the presence of a broad range of extracellular [Ca^{2+}] (1 nM to 10 mM) under symmetrical Na^+ condition. This resulted in an IC_{50} of 319 µM (95 % CI: 192–692 µM) for I_{inst}, and 132 µM (95 % CI: 70–350 µM) for I_{ss} (Fig. 3B). The inhibition by X^{2+} appeared to be limited to the extracellular side, as the presence of 1 mM free Ca^{2+} in the intracellular recording solution did not have any apparent effects on the current phenotype (Fig. S5A).

We hypothesised that the net negative charge around the putative EEKE SF of NALCN (Fig. 3C) influences the sensitivity of X^{2+} block, analogous to what has been demonstrated for Na_Vs and Ca_Vs (*28, 29*). To test this notion directly, we substituted eight charged side chains in the putative SF region of NALCN with alanine and compared the effects of removing X^{2+} between wild-type (WT) and mutant channel complexes expressed in *Xenopus laevis* oocytes. While the WT channel complex showed a large increase (15-fold) in inward currents when X^{2+} (1.8 mM Ca^{2+} and 1 mM Mg^{2+} in ND96) were removed (Fig. 3D-E), the alanine mutations affected the complex's sensitivity to X^{2+} removal to varying degrees. E280A, E554A and D1390A showed drastically reduced current increase (1.5-fold), D558A, E1119A and E1389A showed moderately reduced current increase (3- to 6-fold), while D561A and K1115A showed WT-like (>10-fold) sensitivity (Fig. 3D-E; S5B). These experiments confirm the direct inhibitory effect of X^{2+} on NALCN and suggest that X^{2+} block the channel by interacting with negatively charged side chains around the putative EEKE SF. The C-terminal tail of NALCN has previously been implicated in an indirect Ca^{2+}-sensing mechanism of NALCN that involves the calcium-sensing receptor (*5*). However, we found that C-terminally truncated NALCN variants (Δ1638–1738 and Δ1570–1738) are as sensitive to X^{2+} as the WT channel (Fig. S5C), indicating that the direct effects of X^{2+} on NALCN are not dependent on its C terminus.

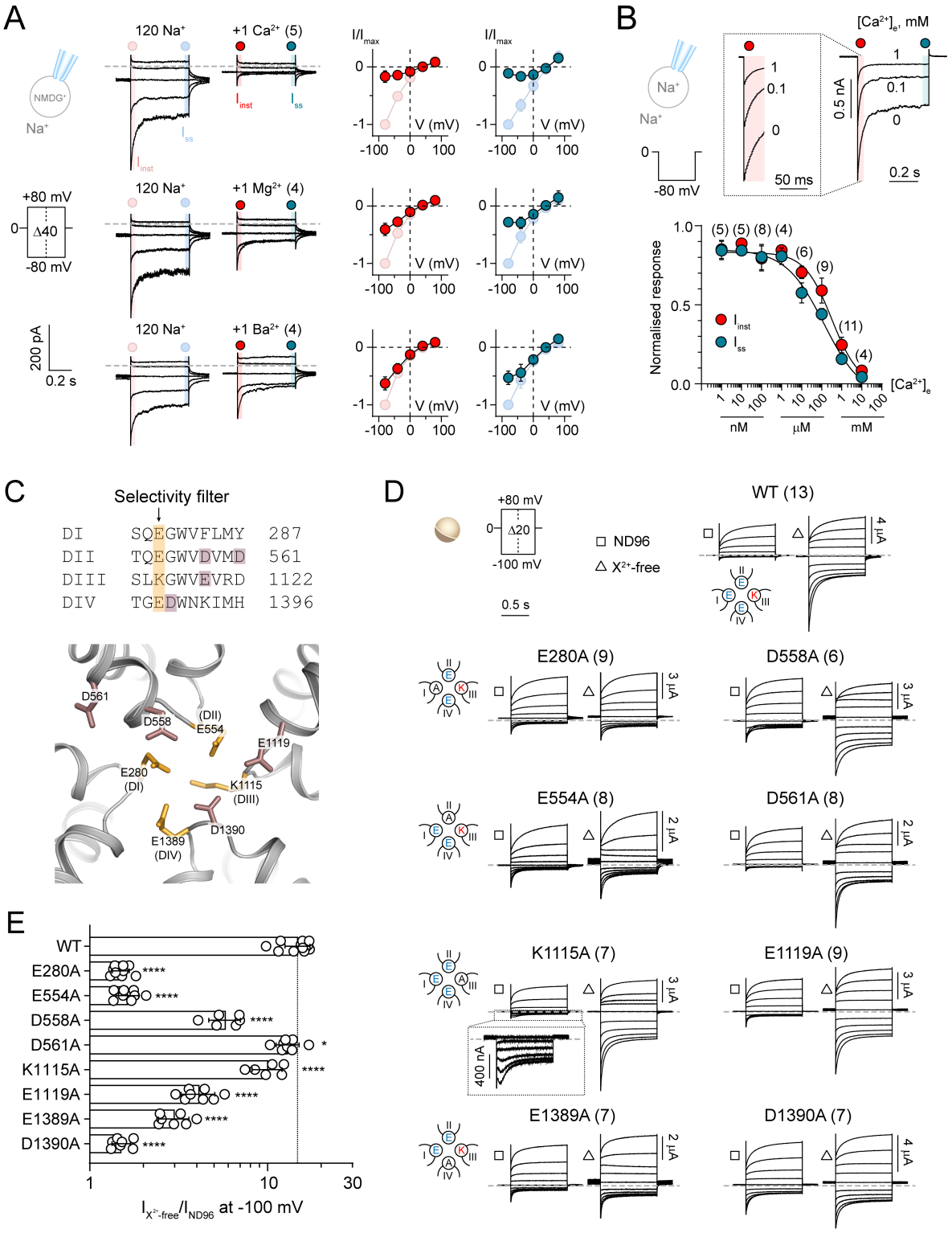

Fig. 3. Divalent cation block of the NALCN channel complex is attenuated by mutations of side chains in the putative SF region. (A) Current responses of HEK-293T cells expressing NALCN*+79+80+155 in the absence and presence of

1 mM Ca^{2+}, Mg^{2+} or Ba^{2+}. Normalised I-V plots illustrate the inhibitory effects of each divalent cation on I_{inst} and I_{ss}. (B) Sample traces of a HEK-293T cell expressing NALCN*+79+80+155 exposed to 0, 0.1 and 1 mM Ca^{2+} under symmetrical Na^{+} condition when stepping from 0 to -80 mV. Inset shows I_{inst} on an expanded time scale. IC_{50} graph shows the potency of Ca^{2+} inhibition on both I_{inst} and I_{ss} of NALCN-mediated current. (C) Top, alignment of the selective filter (SF) region from the four homologous domains in NALCN. The putative SF motif EEKE is highlighted in orange and other negatively charged residues selected for charge neutralisation are highlighted in dark pink. Bottom, homology model of the putative SF region of NALCN based on the structure of $Ca_V1.1$ (PDB ID: 5GJV). (D) Representative currents from *Xenopus laevis* oocytes expressing WT NALCN or alanine mutants in response to step protocols from +80 to -100 mV (HP=0 mV) in the presence (ND96; 1.8 mM Ca^{2+} and 1 mM Mg^{2+}) and absence of divalent cations (X^{2+}-free). (E) Fold-increase in inward current elicited at -100 mV for WT NALCN and SF alanine mutants in response to removal of divalent cations. Data are shown as mean ± SD; *, $p<0.05$; ****, $p<0.0001$; One-way ANOVA, Dunnett's test (against WT); grey dashed lines indicate 0 nA; numbers in parentheses indicate number of individual cells used for recordings. See Fig. S3.

Delineating the molecular basis of voltage sensitivity in NALCN

The reduced number of positively charged side chains in the S4 segments of the VSDs of NALCN (Fig. 4A) has previously been suggested to be the cause of its lack of voltage sensitivity(*4*). Here, however, we observed clear voltage-dependence in the NALCN channel complex (Fig. 1). A similar observation has recently been reported when NALCN and FAM155A were co-expressed in the neuronal cell line NG108-15, which endogenously expresses UNC79 and UNC80 (*30*). To determine the basis of this voltage sensitivity, we mutated positively charged side chains in S4 to glutamine. We found that neutralising most, if not all S4 positive charges in VSDI (R146Q, R152Q and R155Q) or VSDII (R481Q, R484Q and K487Q) resulted in channels that did not respond to voltage pulses at HP of 0 mV, but were still sensitive to depolarising pulses from a HP of -100 mV (Fig. 4B and S6A-C). In contrast, robust WT-like currents were still elicited in neutralised VSDIII (R989Q, R992Q and R995Q) and IV (R1310Q) mutants (Fig. 4B), indicating that the S4 segments in domains III and IV are not essential for the voltage sensitivity of NALCN. Next, we examined the function of single and double charge-neutralising mutations in VSDI and II. Most single and double VSDI mutants exhibited WT-like voltage sensitivity (Fig. 4C), activation time constants (when stepping from 0 to +80 mV in ND96; Fig. 4E), and deactivation time constants (when stepping from 0 to -100 mV in X^{2+}-free buffer; Fig. 4F). While the R143Q+R146Q mutant exhibited WT-like voltage sensitivity (Fig. 4C), it had significantly larger activation time constants than WT (Fig. 4E). The R146Q+R152Q, like the triple R146Q+R152Q+R155Q mutant, did not respond to voltage pulses at HP of 0 mV (Fig. 4C), but was still sensitive to depolarising pulses from a HP of -100 mV (Fig.

S6A-B). These results indicate that the presence of two arginine residues in the middle of the VSDI is critical for voltage sensitivity. In VSDII, the R481Q mutation, but not the R484Q and K487Q single mutations, exhibited altered current kinetics compared to WT (Fig. 4D-E). R481Q showed significantly larger activation time constants when stepping from 0 to +80 mV in ND96 (Fig. 4E). Moreover, out of the 20 VSD mutations tested, R481Q is the only mutation that significant slowed the deactivation time constants when stepping from 0 to -100 mV under the X^{2+}-free condition (Fig. 4F). Neutralising an additional VSDII charge on the background of R481Q rendered the channel irresponsive to voltage pulses at HP of 0 mV (Fig. 4D-E and S6A-B). Taken together, these results suggest that charged residues in both VSDI and II of NALCN are involved in voltage sensing. Supporting evidence for the intrinsic voltage dependence of VSDI originates from the finding that isolated NALCN VSDI generates voltage-dependent currents (Fig. S6D), reminiscent of what is observed with the isolated VSD of *Shaker* potassium channel(*31*).

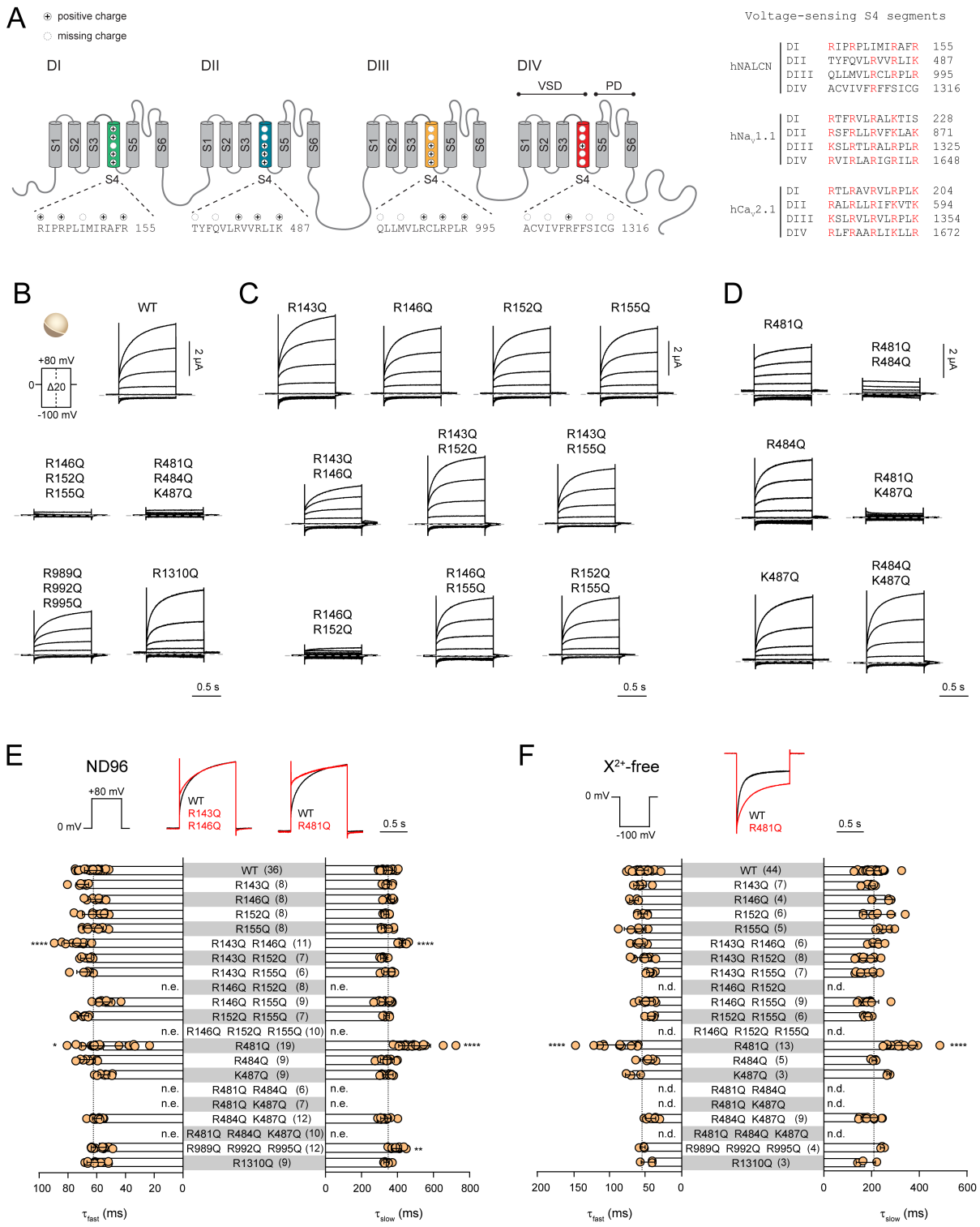

Fig. 4. NALCN voltage sensitivity primarily arises from S4 charges in domains I and II. (A) Left, schematic illustration of the structural topology of NALCN, which consists of four domains (DI–IV) connected via intracellular linkers. Each

domain contains six transmembrane segments (S1–S6), with S1–S4 forming the voltage-sensing domains (VSDs) and S5–S6 forming the pore domains (PDs). The S4 segments typically carry several positively charged residues important in voltage sensing. The conserved and missing (compared to canonical VSDs) positively charged residues in each S4 segment of NALCN is highlighted. Right, alignment of the S4 segments of the four homologous domains in hNALCN, $hNa_V1.1$ and $hCa_V2.1$. Positively charged sides chains are highlighted in red. (B) Current traces and I_{ss}-V plots from *Xenopus laevis* oocytes expressing WT and charge-neutralised mutants in S4 of DI-IV using the indicated protocol. (C-D) Representative traces of single and double charge-neutralised mutants in S4 of VSDI (C) and II (D). (E-F) Slow and fast time constants of depolarisation-elicited currents (0 to +80 mV) in ND96 (E) and hyperpolarisation-elicited currents (0 to -100 mV) in X^{2+}-free buffer (F) for WT and VSD mutants. Superimposed traces of WT (black) and selected VSD mutants (red) are shown above the bar graphs. Data are shown as mean ± SD; *, $p<0.05$; **, $p<0.01$ ****, $p<0.0001$; One-way ANOVA, Dunnett's test (against WT); n.e., no effect; n.d.; not determined; grey dashed lines indicate 0 nA; numbers in parentheses indicate number of individual cells used for recordings.

Discussion

UNC79, UNC80 and FAM155A are crucial for NALCN function

Two decades have passed since NALCN was first cloned, but functional expression of the channel in heterologous systems is still hampered by issues such as low levels of current (*14, 18, 32*) or absence of NALCN-specific currents (*19-21, 23*). Given the ample evidence supporting overlapping spatiotemporal gene expression profiles for NALCN, UNC79, UNC80 and FAM155A in *Drosophila* and mouse (*8, 33*), their functional interdependence in *Drosophila* (*6, 34*), *C. elegans* (*11, 12, 35, 36*) and mouse (*5, 22*) and the physical interactions between these proteins *in vitro* and *in vivo* (*5, 12, 22*), we set out to test the effect of co-expressing these proteins in different heterologous systems. We found that the robust, reproducible functional expression of NALCN is critically dependent on the presence of UNC79, UNC80 and FAM155A/B (Fig. 1A and S1).

UNC79 and UNC80 are widely expressed in the brain, where they form a complex with NALCN and regulate its localisation and function (*5, 11, 34*). While UNC79 is not absolutely required for NALCN activity in mouse hippocampal neurons (NALCN-like currents were observed in the absence of UNC79 (*5*)), both proteins are needed for NALCN function in *Drosophila* (*34*), the neuronal cell line NG108-15 (*30*), HEK-293T cells and *Xenopus laevis*

oocytes (Fig. 1 and S1), highlighting potential interspecies differences in the regulatory roles of these proteins. FAM155A is pivotal for the axonal localisation of NALCN in *C. elegans* (*12*). Based on the proposed ER residency of the *C. elegans* and mouse homologues (*12*), it was suggested that FAM155A acts as a chaperone to facilitate NALCN folding and delivery to the cell membrane. By contrast, we were able to detect plasma membrane localisation of the human FAM155A, even when expressed alone (Fig. 1D). Whether this discrepancy in subcellular localisation is due to species differences requires further investigation. Overall, our data clearly indicate that NALCN function and not membrane localisation *per se*, is critically dependent on the presence of UNC79, UNC80 and FAM155. Furthermore, the co-immunoprecipitation of UNC79, UNC80 and FAM155A with NALCN (Fig. S2B) reinforces the notion that NALCN predominantly functions in complex with other proteins (*26*).

NALCN is the voltage-sensing, pore-forming subunit of the complex

NALCN was considered to be voltage-insensitive due to the reduced number of voltage-sensing residues in the S4 segments compared to typical VGICs. Here, we found that NALCN, when co-expressed with UNC79, UNC80 and FAM155, exhibits an unusual modulation by membrane voltage (Fig. 1). This highlights how voltage sensor domains can, depending on the context, contribute to gating in previously unanticipated ways and thus contributes to our understanding of how this widely encountered motif can modulate ion channel function (*37*). We show that the voltage dependence originates from positively charged residues in the S4 segments of DI and II of NALCN, as charge-neutralising substitutions affected voltage sensitivity (Fig. 4). NALCN had been suggested to be a non-selective cation channel that poorly discriminates between X^+ and X^{2+}. This lack of ion selectivity is often attributed to the EEKE SF motif of NALCN, which is a hybrid between the Na^+-selective DEKA and the Ca^{2+}-selective EEEE. Here, we found that NALCN is moderately selective among the permeable X^+, but does not conduct X^{2+}. The X^+ selectivity profile is altered when the EEKE motif was mutated to DEKA (Fig. 2C). Furthermore, some charge-neutralising mutations around the putative channel pore also affected current rectification and phenotype (Fig. 3D and S5B). For instance, the K1115A mutant displays a unique “hooked” phenotype (Fig. 3D), consistent with the notion that this side chain lines the ion permeation pathway. Taken together, our results strongly support the idea for NALCN to be the voltage-sensing, pore-forming subunit of the complex.

The NALCN channel complex reconstitutes the extracellular [Ca^{2+}]-sensitive NSCC

A non-selective cation current (NSCC) that is activated by the lowering of extracellular [Ca^{2+}] ([Ca^{2+}]$_e$) has been detected in different types of neurons, such as the chick dorsal root ganglia (*38*), mouse hippocampal (*5, 39*), neocortical nerve terminals (*40*) and dopaminergic neurons (*9*). The NSCC depolarises the RMP, allowing the continuous firing of action potentials. The mechanism(s) underlying this phenomenon are not well understood, but the NALCN channel complex may play a role, as NALCN- and UNC79-knockout neurons are insensitive to drops in [Ca^{2+}]$_e$ (*5, 9*). This NALCN-mediated effect has been suggested to occur via an indirect mechanism that is initiated and transduced by the G protein-coupled Ca^{2+}-sensing receptor (CaSR) (*5*). Here, however, we show that the NALCN channel complex-mediated current, without co-expression of GPCRs, is directly blocked by [Ca^{2+}]$_e$, as alanine mutations of several negatively charged residues in the putative pore of NALCN markedly reduced the sensitivity to [Ca^{2+}]$_e$ (Fig. 3D-E). Furthermore, the NALCN channel complex displays strikingly similar biophysical properties compared to the neuronal NSCC: (1) marked increase in inward Na^+ current (>10-fold; Fig. 1 and 3) following the reduction in [Ca^{2+}]$_e$, with a similar sensitivity to [Ca^{2+}]$_e$ (*5, 39, 40*); (2) selective permeability to small X^+, with a small preference for Na^+ over K^+, followed by Cs^+ (Fig. 2) (*39*); (3) insensitivity to TTX (*1-3*) and (4) inhibition by polyvalent cations in the rank order of potency: Gd^{3+}>Ca^{2+}>Mg^{2+} and Ba^{2+} (Fig. 1C and 3A) (*38, 39*).

Physiological implications

The contribution of NALCN to the RMP of neurons, and hence their excitability is undisputed. To perform the task as a regulator of the RMP, it is necessary for NALCN to respond dynamically to the potential difference across the plasma membrane. The unique gating behaviour of the NALCN channel complex, along with the modulation by extracellular X^{2+} through a direct pore-blocking mechanism, accentuate its suitability to perform this task. The constitutive activity of the complex implies that a tonic inward Na^+ conductance will be present even at rest, which may contribute to the depolarisation of the RMP. While this Na^+ conductance is likely to be small in the presence of normal [Ca^{2+}]$_e$ and [Mg^{2+}]$_e$, it is expected to increase considerably following reductions in [Ca^{2+}]$_e$, such as during repetitive chemical or electrical stimulation, or under pathophysiological conditions (*17*), thus lowering the threshold for action potential generation. As such, the NALCN complex is predicted to act as an X^{2+} sensor that directly finetunes neuronal excitability in response to fluctuations of [X^{2+}]$_e$. Furthermore, the differential modulation of NALCN function by voltage means that the NALCN complex undergoes partial deactivation in response to hyperpolarisation, which would allow Na^+ influx to counter the negative shift in membrane potential. By contrast, during prolonged depolarisation, K^+ ions would leave the cell, contributing to the repolarisation of the membrane potential. Overall, we postulate that the NALCN complex functions as a thermostat (or rheostat) that maintains the RMP at a desired value to determine the intrinsic excitability of a neuron.

Materials and Methods

Molecular biology

Human NALCN*, UNC-79*, UNC-80*, FAM155A*, FAM155A• and FAM155B*, and mouse FAM155A* complementary DNAs (cDNAs; * indicates the C-terminal -eGFP-2×FLAG tag; • indicates the C-terminal -MBP-2×FLAG tag) cloned between HindIII and XhoI sites in a modified pCDNA3.1$^{(+)}$ vector containing 3′-*Xenopus* globin UTR and a polyadenylation signal, were generated using custom gene synthesis with codon optimization for *Homo sapiens* (GeneArt, Thermo Fisher Scientific). The tags were removed using the Q5 Site-Directed Mutagenesis Kit (New England Biolabs) to generate wild-type, untagged constructs. The rat NALCN construct was a kind gift from Dr. Dejian Ren at the University of Pennsylvania and was cloned into the same modified pCDNA3.1$^{(+)}$ vector between KpnI and XhoI sites. NALCN pore mutants (Fig. 2 and 3) and non-sense mutations bearing UNC80 variants (Fig. S3 and S4) were generated with site-directed mutagenesis using custom-designed primers (Eurofins Genomics) and PfuUltra II Fusion HS DNA Polymerase (Agilent Technologies). Truncated NALCN, UNC-79*, UNC-80* and FAM155A* constructs (Fig. S3, S4 and S5) were generated using the Q5 Site-Directed Mutagenesis Kit. The sequences of purified plasmid DNAs from transformed *E. coli* were verified by Sanger DNA sequencing (Eurofins Genomics). For expression in *Xenopus laevis* oocytes, plasmid DNAs were linearized with XbaI restriction enzyme, from which capped RNAs were synthesised using the T7 mMessage mMachine Kit (Ambion). For expression in HEK-293T cells, plasmid DNAs purified using the NucleoBond Xtra Midi Plus kit (Macherey-Nagel) were used.

Two-electrode voltage-clamp electrophysiology

Ovarian lobes were surgically removed from female *Xenopus laevis* frogs anaesthetized in 0.3 % tricaine (procedure approved by the Danish Veterinary and Food Administration; license number: 2014-15-0201-0031), divided into smaller clumps, and defolliculated by shaking at 200 rpm, 37 °C in OR2 (in mM: 82.5 NaCl, 2.5 KCl, 1 $MgCl_2$, 5 HEPES; pH 7.4 with NaOH) containing 1 mg/mL of Type I collagenase (Worthington Biochemical Corporation). Healthy-looking stage V-VI oocytes were isolated and injected with 60–70 ng of RNA in a volume of 41–46 nL using a Nanoliter 2010 injector (World Precision Instruments). The NALCN, UNC-79, UNC-80 and FAM155A RNAs were mixed in a ratio of 3:1:1:1. The same ratio was used when NALCN was replaced with rNALCN and when FAM155A was replaced with FAM155B or mFAM155A (Fig. S1B). When one or more constructs are excluded (Fig. S1A), equivolume of nuclease-free water was added to keep the concentration of each RNA constant across different combinations. Injected cells were incubated in OR3 (50 % (v/v) Leibovitz's L-15 medium (Gibco), 1 mM glutamine, 250 µg/mL gentamicin, 15 mM HEPES; pH 7.6 with NaOH) at 18 °C, 140 rpm. Four to five days after RNA injection,

two-electrode voltage-clamp measurements were performed on oocytes continuously perfused in ND96 recording solution (in mM: 96 NaCl, 2 KCl, 1 $MgCl_2$, 1.8 $CaCl_2$, 5 HEPES; pH 7.4 with NaOH) or divalent cation-free ND96 (in mM: 96 NaCl, 2 KCl, 5 HEPES; pH 7.4 with NaOH) at room temperature using a Warner OC-725C Oocyte Clamp amplifier (Warner Instrument Corp, USA). Data were acquired using the pCLAMP 10 software (Molecular Devices) and a Digidata 1550 digitizer (Molecular devices), sampled at 10 kHz. Electrical powerline interference was filtered with a Hum Bug 50/60 Hz Noise Eliminator (Quest Scientific). Recording microelectrodes with resistances around 0.2–1.0 MΩ were pulled from borosilicate glass capillaries (Harvard Apparatus) using a P-1000 Flaming/Brown Micropipette Puller System (Sutter Instrument) and were filled with 3 M KCl.

HEK-293T cell culture and transfection

Human embryonic kidney (HEK-293T) cells were grown in DMEM (Thermo Fisher Scientific) supplemented with 10 % fetal bovine serum (Thermo Fisher Scientific) and 1% penicillin-streptomycin (10, 000 U/mL, Thermo Fisher Scientific) at 37 °C in a 5 % CO_2 humidified growth incubator. Cells between passage 6 to 20 were used for experiments and were tested for mycoplasma (Eurofins Genomics) five times throughout this study. For patch clamp experiments, cells reaching 40–60 % confluency in 35 mm cell culture dishes were transiently transfected with constructs of interest using LipoD293 ver. II (tebu-bio) or PEI 25K (Polysciences) 20 to 24 hours before recording. Depending on the transfection reagent used, a total of 2.5 µg (for LipoD293) or 5 µg (for PEI) of cDNAs were used. The NALCN*, UNC-79, UNC-80 and FAM155A cDNAs were mixed in the mass ratio of 2:1:1:1. When one or more constructs are excluded from the combination, equal amount of empty vector was added to keep the total cDNA amount constant. For mock-transfected cells, empty vector and eGFP were mixed in a 24:1 ratio. For Western blot experiments (Fig. 1D, S2A and S4), cells reaching 20–40 % confluency in 35 mm cell culture dishes were transiently transfected with constructs of interest using LipoD293 two days before the cells were harvested. A total of 0.8 µg of cDNAs was used, with the NALCN*, UNC-79, UNC-80 and FAM155A cDNAs mixed in the mass ratio of 1:1:1:1. For co-immunoprecipitation experiments (Fig. S2B), ~2 to 2.5 million HEK-293T cells were plated on 100 mm cell culture dishes ~30 hours before transfection. A total of 12–20 µg of DNA was used, with the NALCN* or 2×FLAG-eGFP-eGFP-2×FLAG, UNC79-2×FLAG, UNC80-2×FLAG and FAM155A• cDNAs mixed in the mass ratio of 1:1:1:1.

Patch Clamp Electrophysiology

On the day of experiment, transfected HEK-293T cells were seeded on poly-L-lysine coated glass cover slips at least three hours before recording. Cells were voltage-clamped at room temperature in the whole-cell configuration using an Axopatch 200B amplifier (Molecular Devices). Data were acquired using the pCLAMP 10 software (Molecular Devices) and an Axon Digidata 1550A digitizer (Molecular Devices) at 10 kHz. Patch pipettes were pulled from Kwik-Fil 1.5/1.12 (OD/ID, in mm) borosilicate glass capillaries (World Precision Instruments), and fire polished to resistances around 3.0–8.5 MΩ. A custom-built glass perfusion tool with four adjacent barrels (OD/ID 0.45/1.60, in mm; CM Scientific) controlled by a MXPZT-300R solution switcher (Siskiyou) was used to rapidly exchange extracellular solutions.

For symmetrical Na^+ condition (Fig. 1A), extracellular solution contained (in mM): NaCl (150), HEPES (10), D-(+)-glucose (30), pH 7.4 with NaOH, ~325 mOsm/L and intracellular solution contained (in mM): NaCl (136), NaF (10), EGTA (5), HEPES (10), Na_2ATP (2), pH 7.2 with NaOH, ~309 mOsm/L. For a more physiological condition (Fig. 1B), extracellular solution contained (in mM): NaCl (150), KCl (5), $CaCl_2$ (0.5), $MgCl_2$ (1.2), HEPES (10), D-(+)-glucose (13), pH 7.4 with NaOH, ~320 mOsm/L and intracellular solution contained (in mM): CsCl (140), CsF (10), EGTA (5), HEPES (10), Na_2ATP (2), pH 7.2 with CsOH, ~304 mOsm/L. For ion selectivity experiments (Fig. 2): (1) involving monovalent cations, the extracellular solution contained (in mM): XCl (150), HEPES (10), D-(+)-glucose was added accordingly to achieve osmolarity ~325 mOsm/L, and the pH was adjusted to 7.4 with XOH, where X indicates the cation of interest; (2) involving divalent cations, the extracellular solution contained (in mM): XCl_2 (110), HEPES (10), D-(+)-glucose was added accordingly to achieve osmolarity ~325 mOsm/L, and the pH was adjusted to 7.4 with $X(OH)_2$, where X indicates the cation of interest; (3) the intracellular solution contained (in mM): NMDG (150), EGTA (5), HEPES (10), Na_2ATP (2), D-(+)-glucose (30), pH 7.2 with HCl, ~310 mOsm/L. For the determination of Ca^{2+} IC_{50} (Fig. 3B), extracellular Na^+ solutions containing 1 nM to 1 mM free Ca^{2+} were made by mixing Ca^{2+}-free stock (in mM: NaCl (150), HEPES (10) and EGTA (5), pH 7.4 adjusted with NaOH) and 1 mM free Ca^{2+}-stock (in mM: NaCl (150), HEPES (10), EGTA (5), $Ca(OH)_2$ (6), pH 7.4 adjust with NaOH) at the ratio calculated according to the WEBMAXC STANDARD calculator (https://web.stanford.edu/~cpatton/webmaxcS.htm). Solution containing 10 mM Ca^{2+} was prepared by adding $CaCl_2$ from a 1 M stock solution. D-(+)-glucose was added accordingly to all extracellular solutions to achieve osmolarity ~325 mOsm/L. The intracellular solution contained (in mM): NaCl (136), NaF (10), EGTA (5), HEPES (10), Na_2ATP (2), pH 7.2 with NaOH, ~309 mOsm/L.

Experiments involving SFK-targeting peptide or compounds (Fig. S1E-F) were performed under symmetrical Na^+ condition. The Src Family Activator peptide (Santa Cruz Biotechnology; catalogue #: sc-3052) was dissolved in nuclease-free water to make a 1 mM stock solution, and was diluted to a final concentration of 1 µM in the intracellular solution (in mM): NaCl (136), NaF (10), EGTA (5), HEPES (10), Na_2ATP (2), pH 7.2 with NaOH, ~309 mOsm/L. The SFK inhibitors PP1 (catalogue #: P0040) and SU 6656 (catalogue #: S9692) were dissolved in sterile-filtered dimethyl sulfoxide (DMSO; Sigma Aldrich, catologue #: D2650) to make 50 mM and 20 mM stock solutions respectively. PP1 and SU 6656 were then diluted to 5 µM in the extracellular solution (in mM): NaCl (150), HEPES (10), D-(+)-glucose (30), pH 7.4 with NaOH, ~325 mOsm/L. The final concentrations of DMSO in the extracellular solutions were around 0.1–0.025 %v/v.

To prevent non-specific leaks from affecting the accuracy of our results, we routinely checked for loose seals by exposing cells to NMDG-only extracellular solution before and/or after experiments (Fig. 2B). Cells that showed steady-state inward current >10 pA at -80 mV in the absence of permeable ions were discarded. Voltage ramp protocol used to determine E_{rev}s (Fig. 2C) is as follows: whole-cell mode was first achieved in symmetrical $NMDG^+$ solutions, and cells were exposed to NaCl solution for 200 ms before a 1-s voltage step (0 to -80 mV) was applied to obtain a steady-state current; at the end of the voltage step, a 200-ms ramp (-80 to +80 mV) was run before returning to 0 mV; cells were allowed to rest in NDMG solution for ~10 s before the same protocol was run in a solution containing a different ion of interest.

Cell surface biotinylation and Western Blots

Cell surface proteins were purified using the Pierce Cell Surface Protein Isolation Kit (Thermo Fisher Scientific) based on manufacturer instructions with a few modifications: (1) washing was performed with ice-cold PBS-CM (in mM: 137 NaCl, 2.7 KCl, 10 Na_2HPO_4, 1.8 KH_2PO_4, 0.1 $CaCl_2$, 1 $MgCl_2$), (2) biotin was dissolved in ice-cold PBS-CM to a final concentration of 1.25 mg/mL; and (3) the quenching buffer consisted of PBS-CM, supplemented with 200 mM glycine. Cells were lysed in lysis buffer (100 mM Tris-HCl, 150 mM NaCl, pH 7.4, 0.1 % SDS, 1 % Triton-X-1000) supplemented with 1:100 Halt Protease Inhibitor Cocktail (Thermo Fisher Scientific) under gentle agitation on ice for 30 min. Denatured samples from both the total lysates and surface fractions were separated on NuPAGE 3-8 % Tris-Acetate protein gels (Thermo Fisher Scientific) at 200 V for 40 min. The HiMark Pre-Stained Protein Standard (30–460 kDa; Thermo Fisher Scientific) was used as protein molecular weight reference. Samples were transferred onto an Invitrolon PVDF membrane activated with 10 % methanol using the iBlot 2 Dry Blotting System (Thermo Fisher Scientific). The membranes were then incubated in blocking buffer (1×TBS supplemented with 4.5 g/L Fish

gelatin, 1 g/L casein, 0.02 % sodium azide) for 1 hr at RT before they were incubated with the primary antibodies (rabbit anti-FLAG (701629; Invitrogen), mouse anti-β-actin (sc-47778; Santa Cruz Biotechnology), mouse anti-Na^+/K^+-ATPase (05-369; EMD Merck Millipore)) at 4 °C overnight. Next, the membranes were washed 5×2 min with TBST (20 mM Tris-HCl, 150 mM NaCl, 0.1 % Tween 20, pH 7.5) and incubated with the secondary antibodies (IRDye 800CW goat-anti-rabbit (925-32211; LI-COR Biosciences) and IRDye 680RD goat-anti-mouse (926-68070; LI-COR Biosciences)) for 1 hr at RT in the dark. Finally, the membranes were washed 5×2 min in TBST before being imaged using a PXi gel imaging station (Syngene).

Co-immunoprecipitation and Western Blots

HEK-293T cells were harvested ~24 hours post transfection and washed twice in ice-cold PBS. Cells were lysed in lysis buffer (100 mM Tris-HCl, 150 mM NaCl, pH 7.4, 0.1 % SDS, 1 % Triton-X-100) supplemented with 1:100 Halt Protease Inhibitor Cocktail (Thermo Fisher Scientific) with end-over-end rotation at 4 °C for 1 hours. Lysates were cleared by centrifugation at 10,000×g for 10 min, after which the supernatant was transferred onto equilibrated GFP-Trap Magnetic Agarose Beads (ChromoTek) with end-over-end rotation at 4 °C for 2 hours. The magnetic beads were washed four times with lysis buffer before incubation in 2×SDS sample buffer (supplemented with 100 mM DTT) at 60 °C for 20 min to elute bound proteins. Samples from cleared total lysates, supernatant (post incubation with magnetic beads), wash and elution steps were detected with the rabbit anti-FLAG (701629; Invitrogen) antibody using the Western blot technique (described in detail above).

Data analysis

Raw current traces were generally filtered at 500–800 Hz (8-pole Bessel low-pass filter) before data analysis. Current traces were subjected to data reduction (substitute average by a factor of 5) for illustration. Data were presented as mean±standard deviation (SD). Statistical comparisons were performed using GraphPad Prism (version 8.1, GraphPad Software) and the specific tests used were mentioned in text where relevant. For ion selectivity experiments performed with Na^+ intracellular solution (Fig. 2A), liquid junction potential (LJP) was measured with reference to the Na^+ intracellular solution and corrected post-recording. The measured LJP values for extracellular $NMDG^+$ and MS^- solutions were -5.3 and 4.2 mV respectively. For ion selectivity experiments performed with $NMDG^+$ intracellular solution (Fig. 2), LJP was measured with reference to the NMDG intracellular solution and corrected post recording. The measured LJP values for extracellular NaCl, LiCl, KCl and CsCl solutions were 4.5, 2.6, 8.4 and 7.4 mV respectively. Relative ion permeabilities (P_{Na}/P_X) were calculated using the Goldman-

Hodgkin-Katz equation $P_{Na}/P_X=\exp(F(E_{rev(Na)}-E_{rev(X)})/RT)$, where F=Faraday's constant, R=gas constant, T=274 K, and E_{rev}s were measured from the -80 to +80 mV ramp (corrected for LJP). The homology model of human NALCN was generated using the Phyre2 Protein Fold Recognition Server; the model based on the Cav1.1 channel (PDB 5GJV) was selected for the presentation shown in Fig. 3C.

References

1. I. M. Raman, A. E. Gustafson, D. Padgett, Ionic currents and spontaneous firing in neurons isolated from the cerebellar nuclei. *The Journal of Neuroscience* **20**, 9004-9016 (2000).
2. A. C. Jackson, G. L. Yao, B. P. Bean, Mechanism of spontaneous firing in dorsomedial suprachiasmatic nucleus neurons. *The Journal of Neuroscience* **24**, 7985-7998 (2004).
3. Z. M. Khaliq, B. P. Bean, Pacemaking in dopaminergic ventral tegmental area neurons: depolarizing drive from background and voltage-dependent sodium conductances. *The Journal of Neuroscience* **30**, 7401-7413 (2010).
4. B. Lu *et al.*, The neuronal channel NALCN contributes resting sodium permeability and is required for normal respiratory rhythm. *Cell* **129**, 371-383 (2007).
5. B. Lu *et al.*, Extracellular calcium controls background current and neuronal excitability via an UNC79-UNC80-NALCN cation channel complex. *Neuron* **68**, 488-499 (2010).
6. M. Flourakis *et al.*, A conserved bicycle model for circadian clock control of membrane excitability. *Cell* **162**, 836-848 (2015).
7. Y. Shi *et al.*, Nalcn is a "leak" sodium channel that regulates excitability of brainstem chemosensory neurons and breathing. *The Journal of Neuroscience* **36**, 8174-8187 (2016).
8. A. Lutas, C. Lahmann, M. Soumillon, G. Yellen, The leak channel NALCN controls tonic firing and glycolytic sensitivity of substantia nigra pars reticulata neurons. *eLife* **5**, e15271 (2016).
9. F. Philippart, Z. M. Khaliq, Gi/o protein-coupled receptors in dopamine neurons inhibit the sodium leak channel NALCN. *eLife* **7**, e40984 (2018).
10. B. C. Lear *et al.*, The ion channel narrow abdomen is critical for neural output of the *Drosophila* circadian pacemaker. *Neuron* **48**, 965-976 (2005).
11. E. Yeh *et al.*, A putative cation channel, NCA-1, and a novel protein, UNC-80, transmit neuronal activity in C. elegans. *PLOS Biology* **6**, e55 (2008).
12. L. Xie *et al.*, NLF-1 delivers a sodium leak channel to regulate neuronal excitability and modulate rhythmic locomotion. *Neuron* **77**, 1069-1082 (2013).
13. S. Gao *et al.*, The NCA sodium leak channel is required for persistent motor circuit activity that sustains locomotion. *Nature Communications* **6**, 6323 (2015).
14. O. Eigenbrod *et al.*, Rapid molecular evolution of pain insensitivity in multiple African rodents. *Science* **364**, 852-859 (2019).
15. C. Koroglu, M. Seven, A. Tolun, Recessive truncating NALCN mutation in infantile neuroaxonal dystrophy with facial dysmorphism. *Journal of Medical Genetics* **50**, 515-520 (2013).
16. M. D. Al-Sayed *et al.*, Mutations in NALCN cause an autosomal-recessive syndrome with severe hypotonia, speech impairment, and cognitive delay. *The American Journal of Human Genetics* **93**, 721-726 (2013).
17. D. Ren, Sodium leak channels in neuronal excitability and rhythmic behaviors. *Neuron* **72**, 899-911 (2011).
18. L. A. Swayne *et al.*, The NALCN ion channel is activated by M3 muscarinic receptors in a pancreatic beta-cell line. *EMBO Reports* **10**, 873-880 (2009).

19. A. Senatore, A. Monteil, J. van Minnen, A. B. Smit, J. D. Spafford, NALCN ion channels have alternative selectivity filters resembling calcium channels or sodium channels. *PLoS One* **8**, e55088 (2013).
20. A. N. Boone, A. Senatore, J. Chemin, A. Monteil, J. D. Spafford, Gd^{3+} and calcium sensitive, sodium leak currents are features of weak membrane-glass seals in patch clamp recordings. *PLoS One* **9**, e98808 (2014).
21. J. M. Egan, C. A. Peterson, W. M. Fry, Lack of current observed in HEK293 cells expressing NALCN channels. *Biochimie Open* **6**, 24-28 (2018).
22. B. Lu *et al.*, Peptide neurotransmitters activate a cation channel complex of NALCN and UNC-80. *Nature* **457**, 741-744 (2009).
23. J. H. Lee, L. L. Cribbs, E. Perez-Reyes, Cloning of a novel four repeat protein related to voltage-gated sodium and calcium channels. *FEBS letters* **445**, 231-236 (1999).
24. A. C. Dolphin, Voltage-gated calcium channels and their auxiliary subunits: physiology and pathophysiology and pharmacology. *The Journal of Physiology* **594**, 5369-5390 (2016).
25. A. Senatore, J. D. Spafford, A uniquely adaptable pore is consistent with NALCN being an ion sensor. *Channels (Austin)* **7**, 60-68 (2013).
26. M. Cochet-Bissuel, P. Lory, A. Monteil, The sodium leak channel, NALCN, in health and disease. *Frontiers in Cellular Neuroscience* **8**, 132 (2014).
27. J. Pei, N. V. Grishin, Cysteine-rich domains related to Frizzled receptors and Hedgehog-interacting proteins. *Protein science : a publication of the Protein Society* **21**, 1172-1184 (2012).
28. J. Yang, P. T. Elllnor, W. A. Sather, J. I. F. Zhang, R. W. Tsien, Molecular determinants of Ca^{2+} selectivity and ion permeation in L-type Ca^{2+} channels. *Nature* **366**, 158-161 (1993).
29. T. Schlief, R. Schönherr, K. Imoto, S. H. Heinemann, Pore properties of rat brain II sodium channels mutated in the selectivity filter domain. *European Biophysics Journal* **25**, 75-91 (1996).
30. M. Bouasse, H. Impheng, Z. Servant, P. Lory, A. Monteil, Functional expression of CLIFAHDD and IHPRF pathogenic variants of the NALCN channel in neuronal cells reveals both gain- and loss-of-function properties. *Scientific Reports* **9**, 11791 (2019).
31. J. Zhao, R. Blunck, The isolated voltage sensing domain of the Shaker potassium channel forms a voltage-gated cation channel. *eLife* **5**, e18130 (2016).
32. H. Funato *et al.*, Forward-genetics analysis of sleep in randomly mutagenized mice. *Nature* **539**, 378 (2016).
33. A. Ghezzi, B. J. Liebeskind, A. Thompson, N. S. Atkinson, H. H. Zakon, Ancient association between cation leak channels and Mid1 proteins is conserved in fungi and animals. *Frontiers in Molecular Neuroscience* **7**, 15 (2014).
34. B. C. Lear *et al.*, UNC79 and UNC80, putative auxiliary subunits of the NARROW ABDOMEN ion channel, are indispensable for robust circadian locomotor rhythms in Drosophila. *PLoS One* **8**, e78147 (2013).
35. M. Jospin *et al.*, UNC-80 and the NCA ion channels contribute to endocytosis defects in synaptojanin mutants. *Current Biology* **17**, 1595-1600 (2007).
36. J. A. Humphrey *et al.*, A putative cation channel and its novel regulator: cross-species conservation of effects on general anesthesia. *Curr Biol* **17**, 624-629 (2007).
37. F. Bezanilla, How membrane proteins sense voltage. *Nature Reviews Molecular Cell Biology* **9**, 323 (2008).
38. J. J. Hablitz, U. Heinemann, H. D. Lux, Step reductions in extracellular Ca^{2+} activate a transient inward current in chick dorsal root ganglion cells. *Biophysical Journal* **50**, 753-757 (1986).
39. Z.-G. Xiong, W.-Y. Lu, J. F. MacDonald, Extracellular calcium sensed by a novel cation channel in hippocampal neurons. *Proceedings of the National Academy of Sciences of the United States of America* **94**, 7012-7017 (1997).
40. S. M. Smith, J. B. Bergsman, N. C. Harata, R. H. Scheller, R. W. Tsien, Recordings from single neocortical nerve terminals reveal a nonselective cation channel activated by decreases in extracellular calcium. *Neuron* **41**, 243-256 (2004).

Acknowledgments:

General: We thank Janne Colding, Cristiana Chirvas and Cristina Bulancea for technical assistance and Drs. Lesley Anson, Harley Kurata, Jianmin Cui and members of the Pless lab for helpful comments on the manuscript. **Funding:** We acknowledge the Carlsberg Foundation (CF16-0504; SAP), the Independent Research Fund Denmark (7025-00097A; SAP) and the Lundbeck Foundation (R252-2017-1671; SAP) for financial support. **Author contributions:** H.C.C., M.W. and S.A.P. designed the research. H.C.C., M.W., C.W. and L.P.R. performed the experiments. H.C.C., M.W., C.W. and L.P.R. analysed the data. S.A.P. supervised the project. H.C.C. and S.A.P. wrote the manuscript with input from all authors. **Competing interests:** There were no competing interests.

Supplementary Materials

Fig. S1

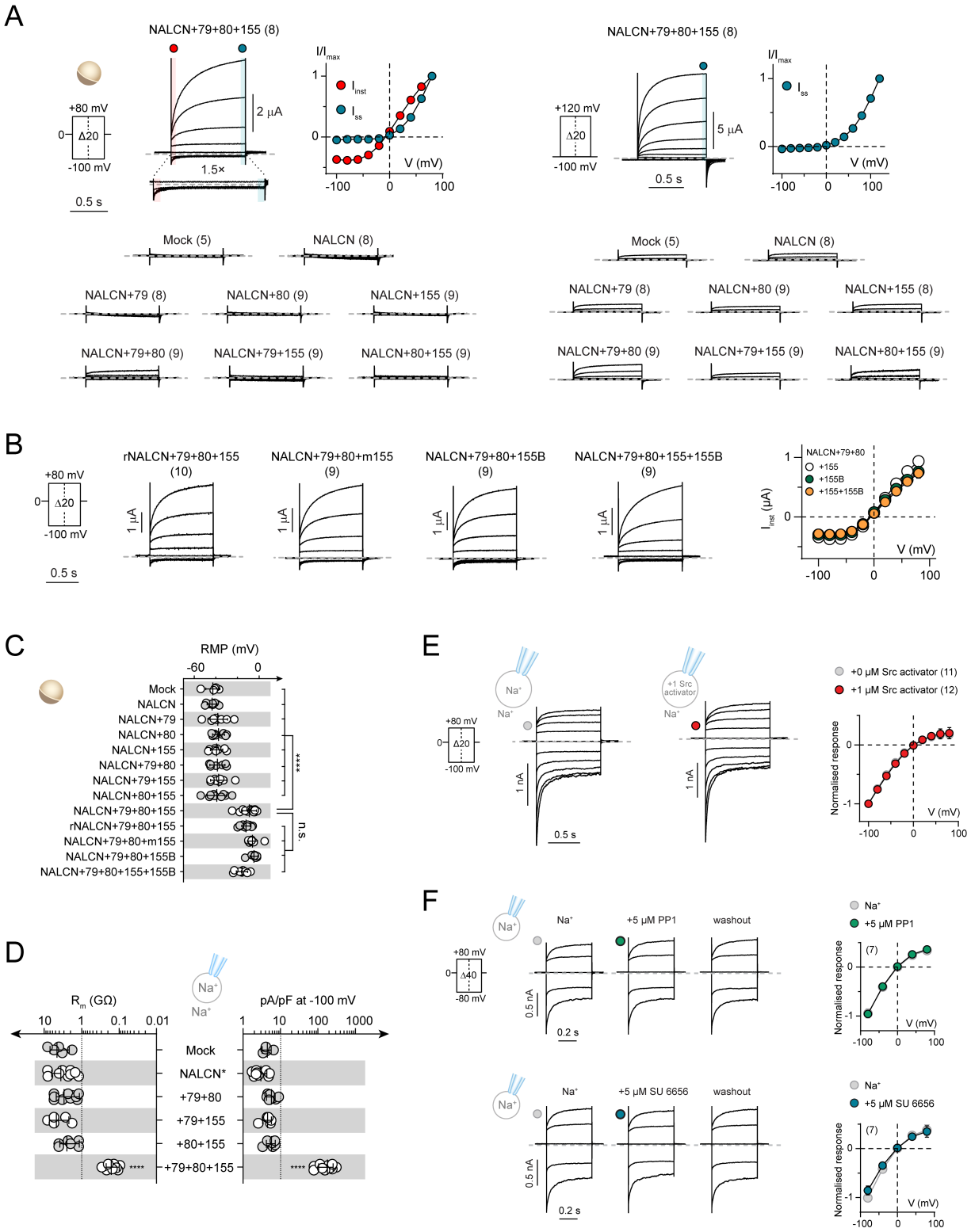

Fig. S1. Basic functional properties of the NALCN channel complex. (A) Representative current traces from *Xenopus laevis* oocytes expressing NALCN alone, or in different combinations with UNC79 (79), UNC80 (80) and FAM155A (155) using a holding potential of 0 mV and -100 mV (left and right panel, respectively). Normalised I-V plots highlighting the different current components of NALCN+79+80+155 are shown next to the current traces. (B) Representative current traces from *Xenopus laevis* oocytes expressing rat NALCN (rNALCN) with UNC79, UNC80 and FAM155A; NALCN with UNC79, UNC80 and mouse FAM155A (m155) or human FAM155B (155B) or 155+155B using the indicated protocol. (C) Resting membrane potential (RMP) of *Xenopus laevis* oocytes expressing the indicated combination of constructs. Data are shown as mean ± SD. n.s, not significant; ****, $p<0.0001$; One-way ANOVA, Dunnett's test (against NALCN+79+80+155). (D) Seal resistances (R_m) and current densities (pA/pF) for HEK cells expressing indicated combination of constructs under symmetrical Na^+ condition. Data are shown as mean ± SD. ****, $p<0.0001$; One-way ANOVA, Dunnett's test (against mock-transfected cells). (E) Whole-cell patch-clamp recordings from HEK-293T cells expressing NALCN-eGFP-2×FLAG (NALCN*) with UNC79, UNC80 and FAM155A under symmetrical Na^+ condition in the absence (grey circle) and presence (red circle) of 1 µM Src activator peptide in the intracellular solution using voltage-step protocols shown on the left. Normalised I-V plots of the instantaneous current (I_{inst}) under both recording conditions are shown on the right. (F) Current responses (left) and normalised I_{inst}-V plots (right) in the absence and presence of 5 µM SFK inhibitor PP1 (top; green circle) or SU 6656 (bottom; blue circle) in the bath solution under symmetrical Na^+ condition. Data are shown as mean ± SD; grey dashed lines indicate 0 nA; numbers in parentheses indicate number of individual cells used for recordings.

Fig. S2

A

Lane #	1	2	3	4	5	6	7	8	9	10	11	12
Protein(s)	N*	N*	79*	79*	80*	80*	155*	155*	N* 79 80 155	N* 79 80 155	N* 79* 80* 155*	N* 79* 80* 155*
TL/S	TL	S	TL	S	TL	S	TL	S	TL	S	TL	S

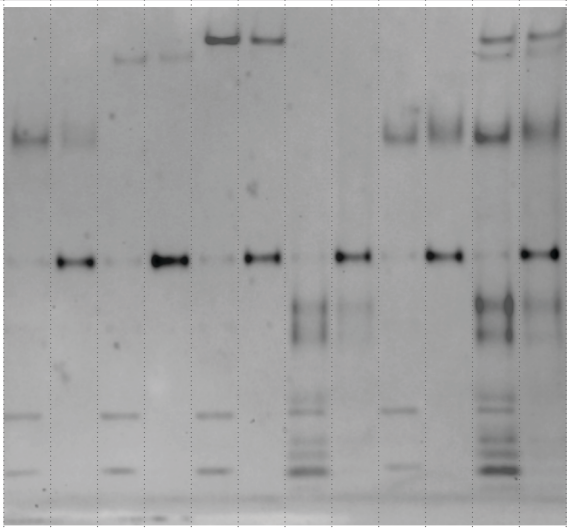

TL = Total lysate N = NALCN 80 = UNC80 * = -eGFP-2×FLAG
S = Surface 79 = UNC79 155 = FAM155A

B

IP: GFP
IB: FLAG

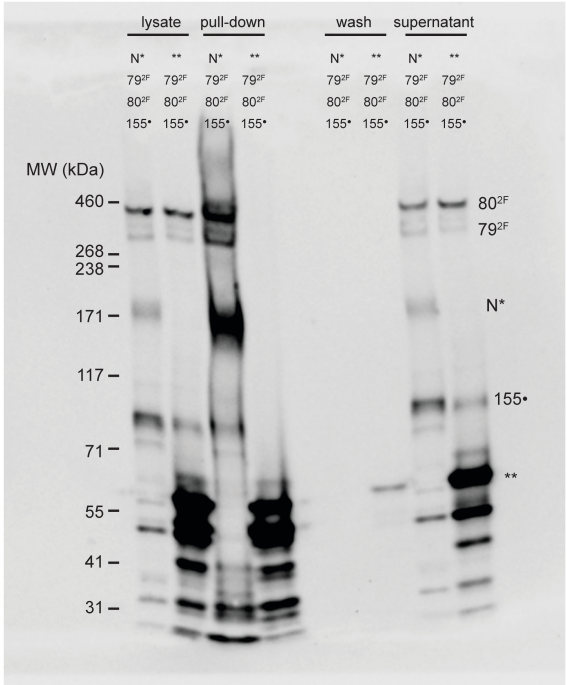

N* = NALCN-eGFP-2×FLAG
79^{2F} = UNC79-2×FLAG
80^{2F} = UNC80-2×FLAG
155• = FAM155A-MBP-2×FLAG
** = 2×FLAG-eGFP-eGFP-2×FLAG
IP = immunoprecipitation
IB = immunoblot
MBP = Maltose-binding protein

Fig. S2. Biochemical analysis of the NALCN channel complex. (A) Uncropped Western blot of total lysate and surface fraction proteins extracted from HEK-293T cells expressing the indicated constructs (shown in Fig. 1D). (B) UNC79, UNC80 and FAM155A were co-immunoprecipitated with NALCN, but not eGFP in HEK-293T cells. NALCN-eGFP-2×FLAG and 2×FLAG-eGFP-eGFP-2×FLAG were immunoprecipitated with anti-GFP nanobody and detected with anti-FLAG antibody. Input of sample on the gel: 1.5 % of total lysate and supernatant, 1 % of the wash and 40 % pull-down of N* or 2% pull down of **, respectively.

Fig. S3

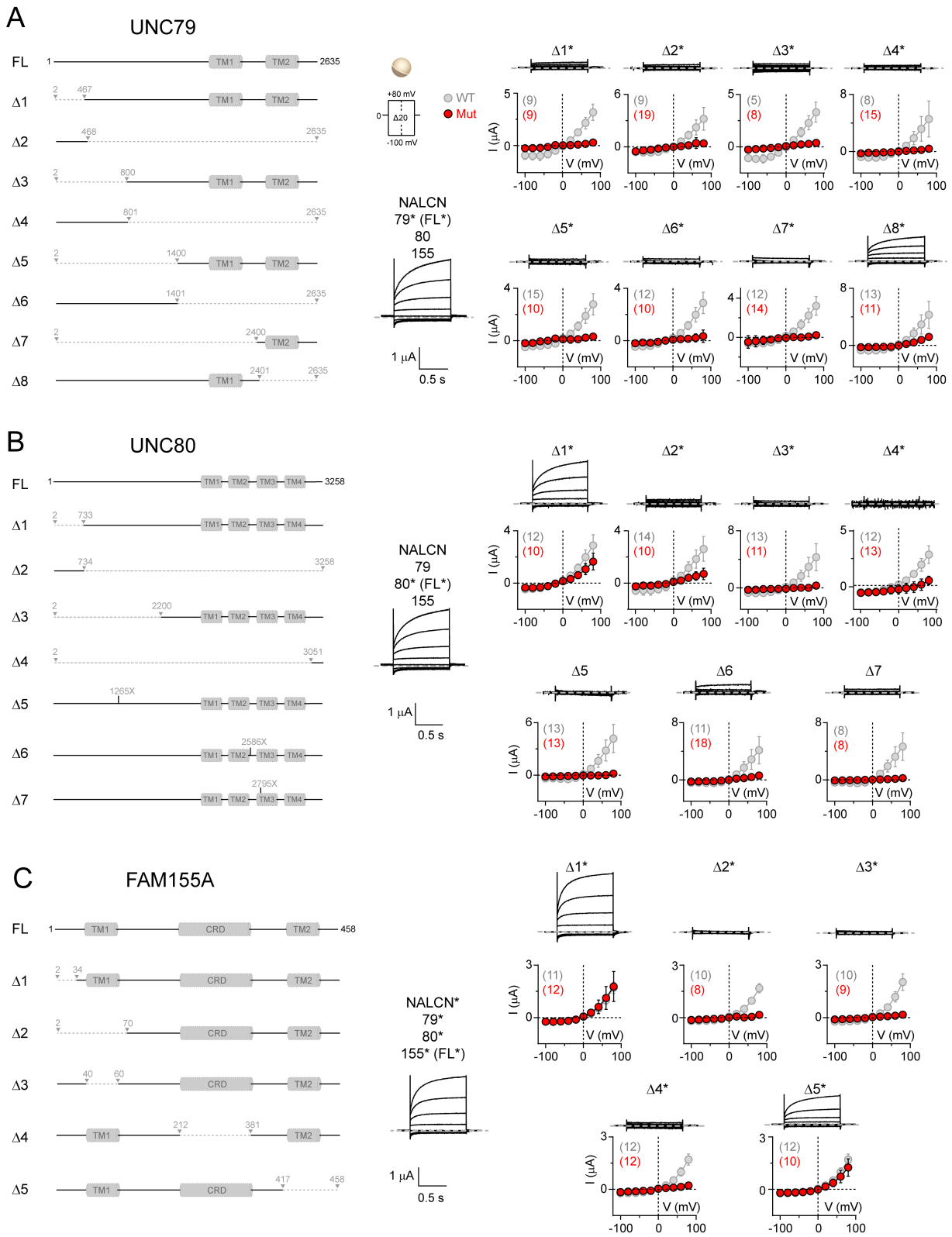
A
UNC79
FL
Δ1
Δ2
Δ3
Δ4
Δ5
Δ6
Δ7
Δ8
TM1
TM2
+80 mV
Δ20
-100 mV
WT
Mut
NALCN
79* (FL*)
80
155
1 μA
0.5 s
I (μA)
V (mV)
B
UNC80
TM3
TM4
1265X
2586X
2795X
NALCN
79
80* (FL*)
155
C
FAM155A
CRD
NALCN*
79*
80*
155* (FL*)

Fig. S3. Truncations of UNC79, UNC80 and FAM155A reveal regions critical to NALCN channel complex function. (A-C) Left panels: Schematic depiction of full-length (FL) proteins, along with a series of truncation constructs (ΔX) of UNC79 (A), UNC80 (B) or FAM155A (C), with putative transmembrane (TM) segments shown in grey. The cartoons are made based on the predicted topology of each protein presented on the UniProt database (UNC79: Q9P2D8; UNC80: Q8N2C7; FAM155A: B1AL88). Right panels: Representative currents traces from *Xenopus laevis* oocytes expressing FL or various truncation constructs using the voltage protocol shown in (A). The I_{ss}-V plots for WT (grey) and truncation constructs (red) are shown below the individual current traces. Data are shown as mean ± SD; grey dashed lines indicate 0 nA; numbers in parentheses indicate number of individual cells used for recordings.

Fig. S4

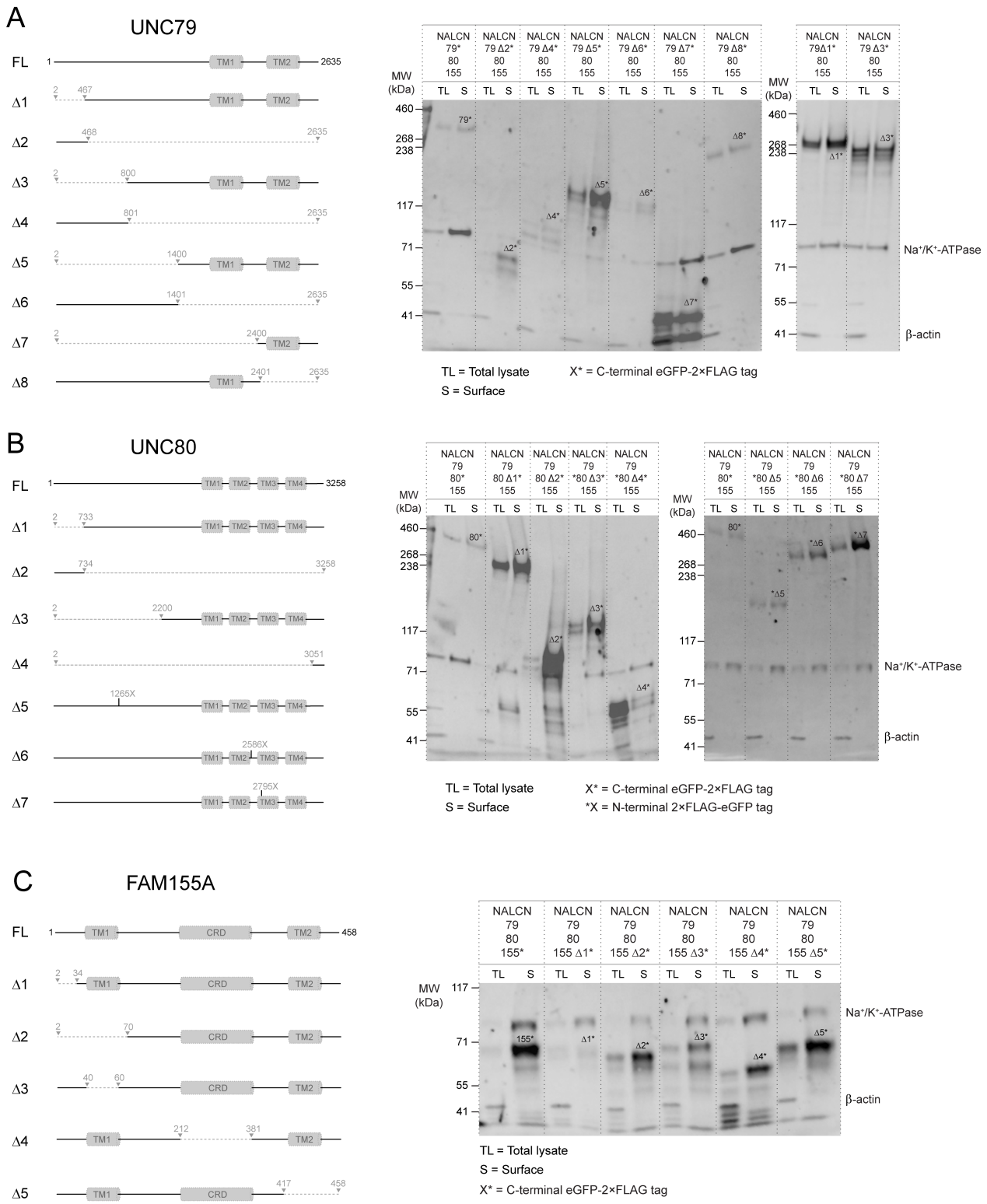
A
UNC79
FL
Δ1
Δ2
Δ3
Δ4
Δ5
Δ6
Δ7
Δ8
TM1
TM2
NALCN 79* 80 155
NALCN 79 Δ2* 80 155
NALCN 79 Δ4* 80 155
NALCN 79 Δ5* 80 155
NALCN 79 Δ6* 80 155
NALCN 79 Δ7* 80 155
NALCN 79 Δ8* 80 155
NALCN 79Δ1* 80 155
NALCN 79 Δ3* 80 155
MW (kDa)
TL S
Na+/K+-ATPase
β-actin
TL = Total lysate
S = Surface
X* = C-terminal eGFP-2×FLAG tag
B
UNC80
TM3
TM4
NALCN 79 80* 155
NALCN 79 80 Δ1* 155
NALCN 79 80 Δ2* 155
NALCN 79 *80 Δ3* 155
NALCN 79 *80 Δ4* 155
NALCN 79 80* 155
NALCN 79 *80 Δ5 155
NALCN 79 *80 Δ6 155
NALCN 79 *80 Δ7 155
TL = Total lysate
S = Surface
X* = C-terminal eGFP-2×FLAG tag
*X = N-terminal 2×FLAG-eGFP tag
C
FAM155A
CRD
NALCN 79 80 155*
NALCN 79 80 155 Δ1*
NALCN 79 80 155 Δ2*
NALCN 79 80 155 Δ3*
NALCN 79 80 155 Δ4*
NALCN 79 80 155 Δ5*
TL = Total lysate
S = Surface
X* = C-terminal eGFP-2×FLAG tag

Fig. S4. Subcellular localisations of truncated UNC79, UNC80 and FAM155A constructs. (A-C) Left panels: Schematic depiction of full-length (FL) proteins, along with a series of truncation constructs (ΔX) of UNC79 (A), UNC80 (B) or FAM155A (C), with putative transmembrane (TM) segments shown in grey. The cartoons are made based on the predicted topology of each protein presented on the UniProt database (UNC79: Q9P2D8; UNC80: Q8N2C7; FAM155A: B1AL88). Right panels: Western blot of total lysate and surface fraction proteins extracted from HEK-293T cells expressing the indicated constructs.

Fig. S5

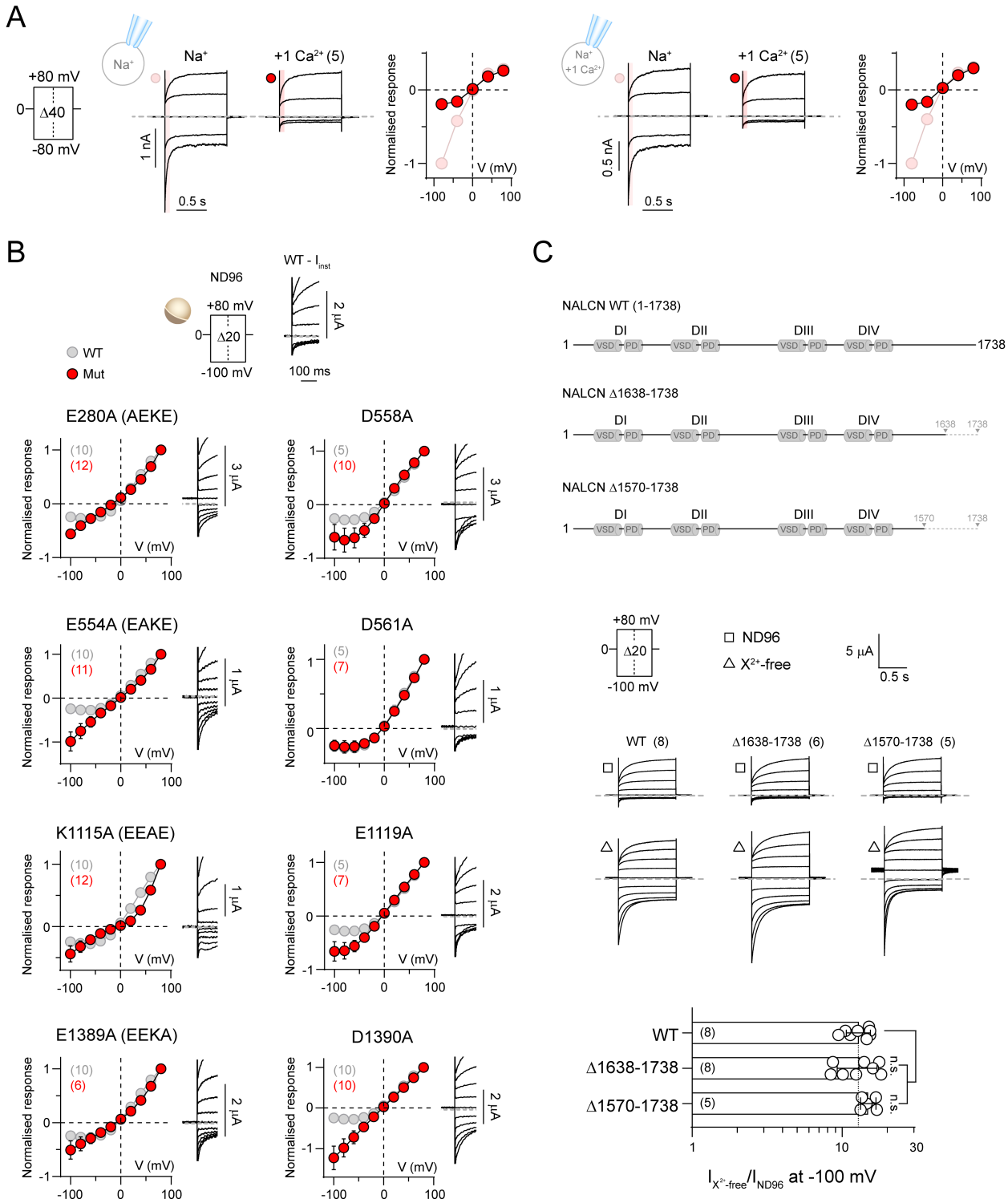
A
+80 mV
0
Δ40
-80 mV
Na+
Na+
+1 Ca2+ (5)
1 nA
0.5 s
Normalised response
V (mV)
Na+
+1 Ca2+
0.5 nA
B
ND96
WT - Iinst
+80 mV
Δ20
-100 mV
2 μA
100 ms
WT
Mut
E280A (AEKE)
D558A
E554A (EAKE)
D561A
K1115A (EEAE)
E1119A
E1389A (EEKA)
D1390A
3 μA
1 μA
2 μA
C
NALCN WT (1-1738)
NALCN Δ1638-1738
NALCN Δ1570-1738
DI
DII
DIII
DIV
VSD
PD
1638
1570
1738
ND96
X2+-free
5 μA
0.5 s
WT (8)
Δ1638-1738 (6)
Δ1570-1738 (5)
n.s.
IX2+-free/IND96 at -100 mV

Fig. S5. The inhibitory effect of X^{2+} on NALCN-mediated current. (A) The effect of extracellular application of 1 mM Ca^{2+} on NALCN current in HEK-293T cells under symmetrical Na^{+} condition in the absence (pink circle) and presence (red circle) of 1 mM free Ca^{2+} in the intracellular solution using voltage-step protocol shown on the left. Normalised I-V plots of the instantaneous current (I_{inst}) under both recording conditions are shown next to the current traces. (B) I_{inst}-V plots (normalised to outward current at +80 mV) from *Xenopus laevis* oocytes expressing WT (grey) and indicated SF alanine mutants (red) recorded in ND96 using the voltage protocol shown on top. Representative current traces highlighting the instantaneous component of WT and SF alanine mutants are shown next to the I-V plots. (C) Top panel: schematic depiction of WT NALCN and C-terminal truncated constructs. Middle panel: representative currents traces from *Xenopus laevis* oocytes expressing WT (1-1738) or C-terminal truncation mutants (Δ1638-1738 and Δ1570-1738) recorded in ND96 (square) and X^{2+}-free buffer (triangle) using the indicated voltage protocol. Bottom panel: Fold-increase in inward current elicited at -100 mV for WT NALCN and truncation mutants in response to removal of divalent cations. Data are shown as mean ± SD; n.s., not significant; One-way ANOVA, Dunnett's test (against WT); grey dashed lines indicate 0 nA; numbers in parentheses indicate number of individual cells used for recordings.

Fig. S6

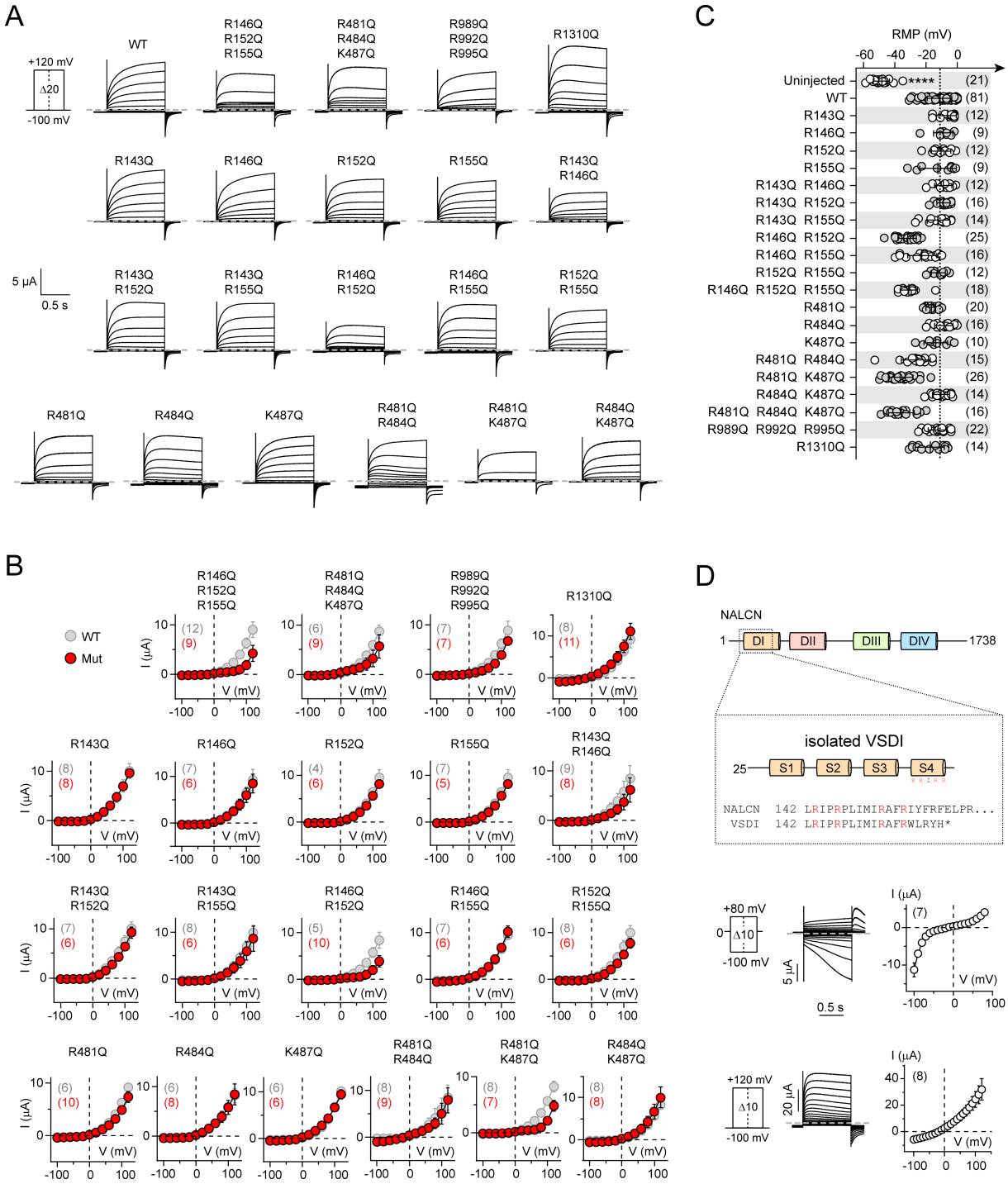
A
+120 mV
Δ20
-100 mV
WT
R146Q R152Q R155Q
R481Q R484Q K487Q
R989Q R992Q R995Q
R1310Q
R143Q
R146Q
R152Q
R155Q
R143Q R146Q
5 μA
0.5 s
R143Q R152Q
R143Q R155Q
R146Q R152Q
R146Q R155Q
R152Q R155Q
R481Q
R484Q
K487Q
R481Q R484Q
R481Q K487Q
R484Q K487Q
C
RMP (mV)
-60 -40 -20 0
Uninjected (21)
WT (81)
R143Q (12)
R146Q (9)
R152Q (12)
R155Q (9)
R143Q R146Q (12)
R143Q R152Q (16)
R143Q R155Q (14)
R146Q R152Q (25)
R146Q R155Q (16)
R152Q R155Q (12)
R146Q R152Q R155Q (18)
R481Q (20)
R484Q (16)
K487Q (10)
R481Q R484Q (15)
R481Q K487Q (26)
R484Q K487Q (14)
R481Q R484Q K487Q (16)
R989Q R992Q R995Q (22)
R1310Q (14)
B
WT
Mut
I (μA)
V (mV)
D
NALCN
1
DI
DII
DIII
DIV
1738
isolated VSDI
25
S1
S2
S3
S4
NALCN 142 LRIPRPLIMIRAFRIYFRFELPR...
VSDI 142 LRIPRPLIMIRAFRWLRYH*
+80 mV
Δ10
-100 mV
5 μA
0.5 s
+120 mV
20 μA

Fig. S6. NALCN voltage sensitivity primarily arises from S4 charges in domains I and II. (A-B) Representative traces (A) and I-V plots (B) from *Xenopus laevis* oocytes expressing WT or charge-neutralised VSDI–IV S4 mutants in response to depolarising voltages from -100 to +120 mV. (C) Resting membrane potentials (RMPs) of uninjected, WT- and VSD mutant-expressing *Xenopus laevis* oocytes. (D) Top panel: schematic depiction of full-length NALCN and the isolated VSDI. Bottom panel: representative traces from *Xenopus laevis* oocytes expressing isolated VSDI in response to two different voltage-step protocols. Data are shown as mean ± SD; ****, $p<0.0001$; One-way ANOVA, Dunnett's test (against uninjected oocytes); grey dashed lines indicate 0 nA; numbers in parentheses indicate number of individual cells used for recordings.

Protein Sequences

>hNALCN (UniProt Accession number: Q8IZF0)
MLKRKQSSRVEAQPVTDFGPDESLSDNADILWINKPWVHSLLRICAIISVISVCMNTPMTFEHYPPLQYVTFTLDTLLMFLYT
AEMIAKMHIRGIVKGDSSYVKDRWCVFDGFMVFCLWVSLVLQVFEIADIVDQMSPWGMLRIPRPLIMIRAFRIYFRFELPRTR
ITNILKRSGEQIWSVSIFLLFFLLLYGILGVQMFGTFTYHCVVNDTKPGNVTWNSLAIPDTHCSPELEEGYQCPPGFKCMDLE
DLGLSRQELGYSGFNEIGTSIFTVYEAASQEGWVFLMYRAIDSFPRWRSYFYFITLIFFLAWLVKNVFIAVIIETFAEIRVQF
QQMWGSRSSTTSTATTQMFHEDAAGGWQLVAVDVNKPQGRAPACLQKMMRSSVFHMFILSMVTVDVIVAASNYYKGENFRRQY
DEFYLAEVAFTVLFDLEALLKIWCLGFTGYISSSLHKFELLLVIGTTLHVYPDLYHSQFTYFQVLRVVRLIKISPALEDFVYK
IFGPGKKLGSLVVFTASLLIVMSAISLQMFCFVEELDRFTTFPRAFMSMFQILTQEGWVDVMDQTLNAVGHMWAPVVAIYFIL
YHLFATLILLSLFVAVILDNLELDEDLKKLKQLKQSEANADTKEKLPLRLRIFEKFPNRPQMVKISKLPSDFTVPKIRESFMK
QFIDRQQQDTCCLLRSLPTTSSSSCDHSKRSAIEDNKYIDQKLRKSVFSIRARNLLEKETAVTKILRACTRQRMLSGSFEGQP
AKERSILSVQHHIRQERRSLRHGSNSQRISRGKSLETLTQDHSNTVRYRNAQREDSEIKMIQEKKEQAEMKRKVQEEELRENH
PYFDKPLFIVGREHRFRNFCRVVVRARFNASKTDPVTGAVKNTKYHQLYDLLGLVTYLDWVMIIVTICSCISMMFESPFRRVM
HAPTLQIAEYVFVIFMSIELNLKIMADGLFFTPTAVIRDFGGVMDIFIYLVSLIFLCWMPQNVPAESGAQLLMVLRCLRPLRI
FKLVPQMRKVVRELFSGFKEIFLVSILLLTLMLVFASFGVQLFAGKLAKCNDPNIIRREDCNGIFRINVSVSKNLNLKLRPGE
KKPGFWVPRVWANPRNFNFDNVGNAMLALFEVLSLKGWVEVRDVIIHRVGPIHGIYIHVFVFLGCMIGLTLFVGVVIANFNEN
KGTALLTVDQRRWEDLKSRLKIAQPLHLPPRPDNDGFRAKMYDITQHPFFKRTIALLVLAQSVLLSVKWDVEDPVTVPLATMS
VVFTFIFVLEVTMKIIAMSPAGFWQSRRNRYDLLVTSLGVVWVVLHFALLNAYTYMMGACVIVFRFFSICGKHVTLKMLLLTV
VVSMYKSFFIIVGMFLLLLCYAFAGVVLFGTVKYGENINRHANFSSAGKAITVLFRIVTGEDWNKIMHDCMVQPPFCTPDEFT
YWATDCGNYAGALMYFCSFYVIIAYIMLNLLVAIIVENFSLFYSTEEDQLLSYNDLRHFQIIWNMVDDKREGVIPTFRVKFLL
RLLRGRLEVDLDKDKLLFKHMCYEMERLHNGGDVTFHDVLSMLSYRSVDIRKSLQLEELLAREQLEYTIEEEVAKQTIRMWLK
KCLKRIRAKQQQSCSIIHSLRESQQQELSRFLNPPSIETTQPSEDTNANSQDNSMQPETSSQQQLLSPTLSDRGGSRQDAADA
GKPQRKFGQWRLPSAPKPISHSVSSVNLRFGGRTTMKSVVCKMNPMTDAASCGSEVKKWWTRQLTVESDESGDDLLDI

>rNALCN (GenBank Accession number: EDM02593.1)
MLKRKQSSRVEAQPVTDFGPDESLSDNADILWINKPWVHSLLRICAIISVISVCMNTPMTFEHYPPLQYVTFTLDTLLMFLYT
AEMIAKMHIRGIVKGDSSYVKDRWCVFDGFMVFCLWVSLVLQVFEIADIVDQMSPWGMLRIPRPLIMIRAFRIYFRFELPRTR
ITNILKRSGEQIWSVSIFLLFFLLLYGILGVQMFGTFTYHCVVNDTKPGNVTWNSLAIPDTHCSPELEEGYQCPPGFKCMDLE
DLGLSRQELGYSGFNEIGTSIFTVYEASSQEGWVFLMYRAIDSFPRWRSYFYFITLIFFLAWLVKNVFIAVIIETFAEIRVQF
QQMWGTRSSTTSTATTQMFHEDAAGGWQLVAVDVNKPQGRAPACLQKMMRSSVFHMFILSMVTVDVIVAASNYYKGENFRRQY
DEFYLAEVAFTVLFDLEALLKIWCLGFTGYISSSLHKFELLLVIGTTLHVYPDLYHSQFTYFQVLRVVRLIKISPALEDFVYK
IFGPGKKLGSLVVFTASLLIVMSAISLQMFCFVEELDRFTTFPRAFMSMFQILTQEGWVDVMDQTLNAVGHMWAPLVAIYFIL
YHLFATLILLSLFVAVILDNLELDEDLKKLKQLKQSEANADTKEKLPLRLRIFEKFPNRPQMVKISKLPSDFTVPKIRESFMK
QFIDRQQQDTCCLFRILPSTSSSSCDNPKRPTVEDNKYIDQKLRKSVFSIRARNLLEKETAVTKILRACTRQRMLSGSFEGQP
AKERSILSVQHHIRQERRSLRHGSNSQRISRGKSLETLTQDHSNTVRYRNAQREDSEIKMIQEKKEQAEMKRKVQEEELRENH
PYFDKPLFIVGREHRFRNFCRVVVRARFNASKTDPVTGAVKNTKYHQLYDLLGLVTYLDWVMITVTICSCISMMFESPFRRVM
HAPTLQIAEYVFVIFMSIELNLKIMADGLFFTPTAVIRDFGGVMDIFIYLVSLIFLCWMPQNVPAESGAQLLMVLRCLRPLRI
FKLVPQMRKVVRELFSGFKEIFLVSILLLTLMLVFASFGVQLFAGKLAKCNDPNIIRREDCNGIFRINVSVSKNLNLKLRPGE
KKPGFWVPRVWANPRNFNFDNVGNAMLALFEVLSLKGWVEVRDVIIHRVGPIHGIYIHVFVFLGCMIGLTLFVGVVIANFNEN
KGTALLTVDQRRWEDLKSRLKIAQPLHLPPRPDNDGFRAKMYDITQHPFFKRTIALLVLAQSVLLSVKWDVEDPVTVPLATMS
VVFTFIFVLEVTMKIIAMSPAGFWQSRRNRYDLLVTSLGVVWVVLHFALLNAYTYMMGACVIVFRFFSICGKHVTLKMLLLTV
VVSMYKSFFIIVGMFLLLLCYAFAGVVLFGTVKYGENINRHANFSSAGKAITVLFRIVTGEDWNKIMHDCMVQPPFCTPDEFT
YWATDCGNYAGALMYFCSFYVIIAYIMLNLLVAIIVENFSLFYSTEEDQLLSYNDLRHFQIIWNMVDDKREGVIPTFRVKFLL
RLLRGRLEVDLDKDKLLFKHMCYEMERLHNGGDVTFHDVLSMLSYRSVDIRKSLQLEELLAREQLEYTIEEEVAKQTIRMWLK
KCLKRIRAKQQQSCSIIHSLRESQQQELSRFLNPPSIETTQPSEDTNANSQDHNTQPESSSQQQLLSPTLSDRGGSRQDAADT
GKPQRKIGQWRLPSAPKPISHSVSSVNLRFGGRTTMKSVVCKMNPMPDTASCGSEVKKWWTRQLTVESDESGDDLLDI

>hUNC79 (UniProt Accession number: Q9P2D8)
MSTKAEQFASKIRYLQEYHNRVLHNIYPVPSGTDIANTLKYFSQTLLSILSRTGKKENQDASNLTVPMTMCLFPVPFPLTPSL
RPQVSSINPTVTRSLLYSVLRDAPSERGPQSRDAQLSDYPSLDYQGLYVTLVTLLDLVPLLQHGQHDLGQSIFYTTTCLLPFL
NDDILSTLPYTMISTLATFPPFLHKDIIEYLSTSFLPMAILGSSRREGVPAHVNLSASSMLMIAMQYTSNPVYHCQLLECLMK
YKQEVWKDLLYVIAYGPSQVKPPAVQMLFHYWPNLKPPGAISEYRGLQYTAWNPIHCQHIECHNAINKPAVKMCIDPSLSVAL
GDKPPPLYLCEECSERIAGDHSEWLIDVLLPQAEISAICQKKNCSSHVRRAVVTCFSAGCCGRHGNRPVRYCKRCHSNHHSNE
VGAAAETHLYQTSPPPINTRECGAEELVCAVEAVISLLKEAEFHAEQREHELNRRRQLGLSSSHHSLDNADFDNKDDDKHDQR
LLSQFGIWFLVSLCTPSENTPTESLARLVAMVFQWFHSTAYMMDDEVGSLVEKLKPQFVTKWLKTVCDVRFDVMVMCLLPKPM
EFARVGGYWDKSCSTVTQLKEGLNRILCLIPYNVINQSVWECIMPEWLEAIRTEVPDNQLKEFREVLSKMFDIELCPLPFSME
EMFGFISCRFTGYPSSVQEQALLWLHVLSELDIMVPLQLLISMFSDGVNSVKELANQRKSRVSELAGNLASRRVSVASDPGRR
VQHNMLSPFHSPFQSPFRSPLRSPFRSPFKNFGHPGGRTIDFDCEDDEMNLNCFILMFDLLLKQMELQDDGITMGLEHSLSKD
IISIINNVFQAPWGGSHTCQKDEKAIECNLCQSSILCYQLACELLERLAPKEESRLVEPTDSLEDSLLSSRPEFIIGPEGEEE
ENPASKHGENPGNCTEPVEHAAVKNDTERKFCYQQLPVTLRLIYTIFQEMAKFEEPDILFNMLNCLKILCLHGECLYIARKDH
PQFLAYIQDHMLIASLWRVVKSEFSQLSSLAVPLLLHALSLPHGADIFWTIINGNFNSKDWKMRFEAVEKVAVICRFLDIHSV
TKNHLLKYSLAHAFCCFLTAVEDVNPAVATRAGLLLDTIKRPALQGLCLCLDFQFDTVVKDRPTILSKLLLLHFLKQDIPALS
WEFFVNRFETLSLEAQLHLDCNKEFPFPTTITAVRTNVANLSDAALWKIKRARFARNRQKSVRSLRDSVKGPVESKRALSLPE
TLTSKIRQQSPENDNTIKDLLPEDAGIDHQTVHQLITVLMKFMAKDESSAESDISSAKAFNTVKRHLYVLLGYDQQEGCFMIA
PQKMRLSTCFNAFIAGIAQVMDYNINLGKHLLPLVVQVLKYCSCPQLRHYFQQPPRCSLWSLKPHIRQMWLKALLVILYKYPY
RDCDISKILLHLIHITVNTLNAQYHSCKPHATAGPLYSDNSNISRYSEKEKGEIELAEYRETGALQDSLLHCVREESIPKKKL
RSFKQKSLDIGNADSLLFTLDEHRRKSCIDRCDIEKPPTQAAYIAQRPNDPGRSRQNSATRPDNSEIPENPAMEGFPDARRPV
IPEVRLNCMETFEVKVDSPVKPAPKEDLDLIDLSSDSTSGPEKHSILSTSDSDSLVFEPLPPLRIVESDEEEETMNQGDDGPS
GKNAASSPSVPSHPSVLSLSTAPLVQVSVEDCSKDFSSKDSGNNQSAGNTDSALITLEDPMDAEGSSKPEELPEFSCGSPLTL
KQKRDLLQKSFALPEMSLDDHPDPGTEGEKPGELMPSSGAKTVLLKVPEDAENPTESEKPDTSAESDTEQNPERKVEEDGAEE
SEFKIQIVPRQRKQRKIAVSAIQREYLDISFNILDKLGEQKDPDPSTKGLSTLEMPRESSSAPTLDAGVPETSSHSSISTQYR
QMKRGSLGVLTMSQLMKRQLEHQSSAPHNISNWDTEQIQPGKRQCNVPTCLNPDLEGQPLRMRGATKSSLLSAPSIVSMFVPA
PEEFTDEQPTVMTDKCHDCGAILEEYDEETLGLAIVVLSTFIHLSPDLAAPLLLDIMQSVGRLASSTTFSNQAESMMVPGNAA
GVAKQFLRCIFHQLAPNGIFPQLFQSTIKDGTFLRTLASSLMDFNELSSIAALSQLLEGLNNKKNLPAGGAMIRCLENIATFM
EALPMDSPSSLWTTISNQFQTFFAKLPCVLPLKCSLDSSLRIMICLLKIPSTNATRSLLEPFSKLLSFVIQNAVFTLAYLVEL
CGLCYRAFTKERDKFYLSRSVVLELLQALKLKSPLPDTNLLLLVQFICADAGTKLAESTILSKQMIASVPGCGTAAMECVRQY
INEVLDFMADMHTLTKLKSHMKTCSQPLHEDTFGGHLKVGLAQIAAMDISRGNHRDNKAVIRYLPWLYHPPSAMQQGPKEFIE
CVSHIRLLSWLLLGSLTHNAVCPNASSPCLPIPLDAGSHVADHLIVILIGFPEQSKTSVLHMCSLFHAFIFAQLWTVYCEQSA
VATNLQNQNEFSFTAILTALEFWSRVTPSILQLMAHNKVMVEMVCLHVISLMEALQECNSTIFVKLIPMWLPMIQSNIKHLSA
GLQLRLQAIQNHVNHHSLRTLPGSGQSSAGLAALRKWLQCTQFKMAQVEIQSSEAASQFYPL

>hUNC80 (UniProt Accession number: Q8N2C7)
MVKRKSSEGQEQDGGRGIPLPIQTFLWRQTSAFLRPKLGKQYEASCVSFERVLVENKLHGLSPALSEAIQSISRWELVQAALP
HVLHCTATLLSNRNKLGHQDKLGVAETKLLHTLHWMLLEAPQDCNNERFGGTDRGSSWGGSSSAFIHQVENQGSPGQPCQSSS
NDEEENNRRKIFQNSMATVELFVFLFAPLVHRIKESDLTFRLASGLVIWQPMWEHRQPGVSGFTALVKPIRNIITAKRSSPIN
SQSRTCESPNQDARHLEGLQVVCETFQSDSISPKATISGCHRGNSFDGSLSSQTSQERGPSHSRASLVIPPCQRSRYATYFDV
AVLRCLLQPHWSEEGTQWSLMYYLQRLRHMLEEKPEKPPEPDIPLLPRPRSSSMVAAAPSLVNTHKTQDLTMKCNEEEKSLSS
EAFSKVSLTNLRRSAVPDLSSDLGMNIFKKFKSRKEDRERKGSIPFHHTGKRRPRRMGVPFLLHEDHLDVSPTRSTFSFGSFS
GLGEDRRGIEKGGWQTTILGKLTRRGSSDAATEMESLSARHSHSHHTLVSDLPDPSNSHGENTVKEVRSQISTITVATFNTTL
ASFNVGYADFFNEHMRKLCNQVPIPEMPHEPLACANLPRSLTDSCINYSYLEDTEHIDGTNNFVHKNGMLDLSVVLKAVYLVL
NHDISSRICDVALNIVECLLQLGVVPCVEKNRKKSENKENETLEKRPSEGAFQFKGVSGSSTCGFGGPAVSGAGDGGGEEGGG
GDGGGGGGDGGGGGGGGGGPYEKNDKNQEKDESTPVSNHRLALTMLIKIVKSLGCAYGCGEGHRGLSGDRLRHQVFRENAQNC
LTKLYKLDKMQFRQTMRDYVNKDSLNNVVDFLHALLGFCMEPVTDNKAGFGNNFTTVDNKSTAQNVEGIIVSAMFKSLITRCA
STTHELHSPENLGLYCDIRQLVQFIKEAHGNVFRRVALSALLDSAEKLAPGKKVEENEQESKPAGSKRSEAGSIVDKGQVSSA
PEECRSFMSGRPSQTPEHDEQMQGANLGRKDFWRKMFKSQSAASDTSSQSEQDTSECTTAHSGTTSDRRARSRSRRISLRKKL
KLPIGKRNWLKRSSLSGLADGVEDLLDISSVDRLSFIRQSSKVKFTSAVKLSEGGPGSGMENGRDEEENFFKRLGCHSFDDHL
SPNQDGGKSKNVVNLGAIRQGMKRFQFLLNCCEPGTIPDASILAAALDLEAPVVARAALFLECARFVHRCNRGNWPEWMKGHH
VNITKKGLSRGRSPIVGNKRNQKLQWNAAKLFYQWGDAIGVRLNELCHGESESPANLLGLIYDEETKRRLRKEDEEEDFLDDS
TVNPSKCGCPFALKMAACQLLLEITTFLRETFSCLPRPRTEPLVDLESCRLRLDPELDRHRYERKISFAGVLDENEDSKDSLH
SSSHTLKSDAGVEEKKEGSPWSASEPSIEPEGMSNAGAEENYHRNMSWLHVMILLCNQQSFICTHVDYCHPHCYLHHSRSCAR
LVRAIKLLYGDSVDSLRESSNISSVALRGKKQKECSDKSCLRTPSLKKRVSDANLEGKKDSGMLKYIRLQVMSLSPAPLSLLI
KAAPILTEEMYGDIQPAAWELLLSMDEHMAGAAAAMFLLCAVKVPEAVSDMLMSEFHHPETVQRLNAVLKFHTLWRFRYQVWP
RMEEGAQQIFKIPPPSINFTLPSPVLGMPSVPMFDPPWVPQCSGSVQDPINEDQSKSFSARAVSRSHQRAEHILKNLQQEEEK
KRLGREASLITAIPITQEACYEPTCTPNSEPEEEVEEVTNLASRRLSVSPSCTSSTSHRNYSFRRGSVWSVRSAVSAEDEEHT
TEHTPNHHVPQPPQAVFPACICAAVLPIVHLMEDGEVREDGVAVSAVAQQVLWNCLIEDPSTVLRHFLEKLTISNRQDELMYM
LRKLLLNIGDFPAQTSHILFNYLVGLIMYFVRTPCEWGMDAISATLTFLWEVVGYVEGLFFKDLKQTMKKEQCEVKLLVTASM
PGTKTLVVHGQNECDIPTQLPVHEDTQFEALLKECLEFFNIPESQSTHYFLMDKRWNLIHYNKTYVRDIYPFRRSVSPQLNLV
HMHPEKGQELIQKQVFTRKLEEVGRVLFLISLTQKIPTAHKQSHVSMLQEDLLRLPSFPRSAIDAEFSLFSDPQAGKELFGLD
TLQKSLWIQLLEEMFLGMPSEFPWGDEIMLFLNVFNGALILHPEDSALLRQYAATVINTAVHFNHLFSLSGYQWILPTMLQVY
SDYESNPQLRQAIEFACHQFYILHRKPFVLQLFASVAPLLEFPDAANNGPSKGVSAQCLFDLLQSLEGETTDILDILELVKAE
KPLKSLDFCYGNEDLTFSISEAIKLCVTVVAYAPESFRSLQMLMVLEALVPCYLQKLKRQTSQVETVPAAREEIAATAALATS
LQALLYSVEVLTRPMTAPQMSRCDQGHKGTTTANHTMSSGVNTRYQEQGAKLHFIRENLHLLEEGQGIPREELDERIAREEFR
RPRESLLNICTEFYKHCGPRLKILQNLAGEPRVIALELLDVKSHMRLAEIAHSLLKLAPYDTQTMESRGLRRYIMEMLPITDW
TAEAVRPALILILKRLDRMFNKIHKMPTLRRQVEWEPASNLIEGVCLTLQRQPIISFLPHLRSLINVCVNLVMGVVGPSSVAD
GLPLLHLSPYLSPPLPFSTAVVRLVALQIQALKEDFPLSHVISPFTNQERREGMLLNLLIPFVLTVGSGSKDSPWLEQPEVQL
LLQTVINVLLPPRIISTSRSKNFMLESSPAHCSTPGDAGKDLRREGLAESTSQAAYLALKVILVCFERQLGSQWYWLSLQVKE
MALRKVGGLALWDFLDFIVRTRIPIFVLLRPFIQCKLLAQPAENHEELSARQHIADQLERRFIPRPLCKSSLIAEFNSELKIL
KEAVHSGSAYQGKTSISTVGTSTSAYRLSLATMSRSNTGTGTVWEQDSEPSQQASQDTLSRTDEEDEENDSISMPSVVSEQEA
YLLSAIGRRRFSSHVSSMSVPQAEVGMLPSQSEPNVLDDSQGLAAEGSLSRVASIQSEPGQQNLLVQQPLGRKRGLRQLRRPL
LSRQKTQTEPRNRQGARLSTTRRSIQPKTKPSADQKRSVTFIEAQPEPAAAPTDALPATGQLQGCSPAPSRKPEAMDEPVLTS
SPAIVVADLHSVSPKQSENFPTEEGEKEEDTEAQGATAHSPLSAQLSDPDDFTGLETSSLLQHGDTVLHISEENGMENPLLSS
QFTFTPTELGKTDAVLDESHV

>hFAM155A (UniProt Accession number: B1AL88)
MTRGAWMCRQYDDGLKIWLAAPRENEKPFIDSERAQKWRLSLASLLFFTVLLSDHLWFCAEAKLTRARDKEHQQQQRQQQQQQ
QQQRQRQQQQQQRRQQEPSWPALLASMGESSPAAQAHRLLSASSSPTLPPSPGDGGGGGGKGNRGKDDRGKALFLGNSAKPVW
RLETCYPQGASSGQCFTVENADAVCARNWSRGAAGGDGQEVRSKHPTPLWNLSDFYLSFCNSYTLWELFSGLSSPNTLNCSLD
VVLKEGGEMTTCRQCVEAYQDYDHHAQEKYEEFESVLHKYLQSEEYSVKSCPEDCKIVYKAWLCSQYFEVTQFNCRKTIPCKQ
YCLEVQTRCPFILPDNDEVIYGGLSSFICTGLYETFLTNDEPECCDVRREEKSNNPSKGTVEKSGSCHRTSLTVSSATRLCNS
RLKLCVLVLILLHTVLTASAAQNTAGLSFGGINTLEENSTNEE

>hFAM155B (UniProt Accession number: O75949. Note an additional Lys at position 372 compared to O75949-1)
MFRGAWMWPGKDAAALTICCCCCCWAPRPSDKPCADSERAQRWRLSLASLLFFTVLLADHLWLCAGARPRARELSSAMRPPWG
AGRERQPVPPRAVLPLPPPPPGEPSAPPGTCGPRYSNLTKAAPAAGSRPVCGGVPEPTGLDAACTKLQSLQRLFEPTTPAPPL
RPPDSLSRAPAEFPSAKKNLLKGHFRNFTLSFCDTYTVWDLLLGMDRPDSLDCSLDTLMGDLLAVVASPGSGAWEACSNCIEA
YQRLDRHAQEKYDEFDLVLHKYLQAEEYSIRSCTKGCKAVYKAWLCSEYFSVTQQECQRWVPCKQYCLEVQTRCPFILPDNEE
MVYGGLPGFICTGLLDTSPKRLETKCCDVQWVSCEAKKKKKFKESEAPKTHQQQFHHSYFHHYHQQYHHYHPHHDPPGRVSNK
PALLPVSGGSRLSPSRIRLCVLVLMLLHTVVSFSSNQGGGGLGLETLPALEEGLTREE

>mFAM155A (UniProt Accession number: Q8CCS2)
MTRGAWMCRQYDDGLKIWLAAPRENEKPFIDSERAQKWRLSLASLLFFTVLLSDHLWFCAEAKLTRTRDKEHHQQQQQQQQQQ
QQQQQQQQQQQQRQQQRQRQQQRQRQQEPSWPALLASMGESSPAAQAHRLLSASSSPTLPPSPGGGGGSKGNRGKNNRSRALF
LGNSAKPVWRLETCYPQGASSGQCFTVESADAVCARNWSRGAAAGEEQSSRGSRPTPLWNLSDFYLSFCNSYTLWELFSGLSS
PSTLNCSLDVVLTEGGEMTTCRQCIEAYQDYDHHAQEKYEEFESVLHKYLQSDEYSVKSCPEDCKIVYKAWLCSQYFEVTQFN
CRKTIPCKQYCLEVQTRCPFILPDNDEVIYGGLSSFICTGLYETFLTNDEPECCDIRSEEQTAPRPKGTVDRRDSCPRTSLTV
SSATRLCPGRLKLCVLVLILLHTVLTASAAQNSTGLGLGGLPTLEDNSTRED

>isolated VSD1 of NALCN
MSDNADILWINKPWVHSLLRICAIISVISVCMNTPMTFEHYPPLQYVTFTLDTLLMFLYTAEMIAKMHIRGIVKGDSSYVKDR
WCVFDGFMVFCLWVSLVLQVFEIADIVDQMSPWGMLRIPRPLIMIRAFRWLRYH

>C-term_-eGFP-2×FLAG_tag
……GGSGGSVSKGEELFTGVVPILVELDGDVNGHKFSVSGEGEGDATYGKLTLKFICTTGKLPVPWPTLVTTLTYGVQCFSRYP
DHMKQHDFFKSAMPEGYVQERTIFFKDDGNYKTRAEVKFEGDTLVNRIELKGIDFKEDGNILGHKLEYNYNSHNVYIMADKQK
NGIKVNFKIRHNIEDGSVQLADHYQQNTPIGDGPVLLPDNHYLSTQSALSKDPNEKRDHMVLLEFVTAAGITLGMDELYKGGS
GGSDYKDDDDKGSGDYKDDDDK

>C-term_-MBP-2×FLAG_tag
……GGSGGSKIEEGKLVIWINGDKGYNGLAEVGKKFEKDTGIKVTVEHPDKLEEKFPQVAATGDGPDIIFWAHDRFGGYAQSGL
LAEITPDKAFQDKLYPFTWDAVRYNGKLIAYPIAVEALSLIYNKDLLPNPPKTWEEIPALDKELKAKGKSALMFNLQEPYFTW
PLIAADGGYAFKYENGKYDIKDVGVDNAGAKAGLTFLVDLIKNKHMNADTDYSIAEAAFNKGETAMTINGPWAWSNIDTSKVN
YGVTVLPTFKGQPSKPFVGVLSAGINAASPNKELAKEFLENYLLTDEGLEAVNKDKPLGAVALKSYEEELAKDPRIAATMENA
QKGEIMPNIPQMSAFWYAVRTAVINAASGRQTVDEALKDAQTNSSSNNNNNNNNNNGGSGGSDYKDDDDKGSGDYKDDDDK